Geochemistry, Geophysics, Geosystems

RESEARCH ARTICLE
10.1029/2020GC009040

Revisiting the Australian-Antarctic Ocean-Continent Transition Zone Using Petrological and Geophysical Characterization of Exhumed Subcontinental Mantle

A. McCarthy[1,2], T. J. Falloon[3], I. Sauermilch[4], J. M. Whittaker[4], K. Niida[5], and D. H. Green[3]

[1]School of Earth Sciences, University of Bristol, Clifton, UK, [2]Now at: Institute for Marine and Antarctic Studies, University of Tasmania, Hobart, Australia, [3]CODES and Earth Sciences, School of Natural Sciences, University of Tasmania, Hobart, Australia, [4]Institute for Marine and Antarctic Studies, University of Tasmania, Hobart, Australia, [5]Hokkaido University Museum, Sapporo, Japan

Key Points:
- Seismic transects along Terre Adélie (East Antarctica) indicate a 50–100 km wide domain of exhumed subcontinental mantle
- Seamount B likely records MORB impregnation of subcontinental mantle at high pressures (≥8 kbar)
- Magnetic anomalies are likely formed by sparse volcanism along an OCT dominated by exhumed mantle

Supporting Information:
- Supporting Information S1

Correspondence to:
A. McCarthy,
anders.mccarthy@bristol.ac.uk;
anders.mccarthy@utas.edu.au

Citation:
McCarthy, A., Falloon, T. J., Sauermilch, I., Whittaker, J. M., Niida, K., & Green, D. H. (2020). Revisiting the Australian-Antarctic ocean-continent transition zone using petrological and geophysical characterization of exhumed subcontinental mantle. *Geochemistry, Geophysics, Geosystems*, *21*, e2020GC009040. https://doi.org/10.1029/2020GC009040

Received 10 FEB 2020
Accepted 31 MAY 2020
Accepted article online 2 JUN 2020

Abstract The final lithospheric breakup of the Australian-Antarctic rift system remains controversial due to sparse geological constraints on the nature of the basement along the ocean-continent transition (OCT) zones. We present new interpretations of multichannel seismic reflection transects and new petrological data of dredged mantle rocks along the East Antarctic margin (Seamount B, offshore Terre Adélie). By combining both data sets, we show that a 50–100 km wide domain of cold and fertile subcontinental mantle was exhumed along the magma-poor Antarctic margin. This study represents only the second locality, along with the Iberia-Newfoundland margins, where the importance of exhumed mantle domains along OCTs can be clearly identified. The dredged peridotites preserve characteristics similar to mantle xenoliths found in syn- to post-rift volcanism at the eastern end of the Australian margin (Victoria and Tasmania), indicating the exhumation of fertile subcontinental mantle during rifting between Australia and Antarctica. Seamount B represents the initial stages of exhumation of cold subcontinental lithosphere along an OCT during rifting. This thick mantle domain was likely affected by melt impregnation at high pressure (8 kbar), leading to the formation of plagioclase-pyroxenites. The combination of continental rifted blocks, a wide domain of volcanic-poor subcontinental mantle and (ultra-) slow spreading is analogous to OCTs from the Jurassic Western Tethys and Iberia-Newfoundland rifted margins. Additionally, evidence of melt stagnation at high pressure suggests that magmatism along the Australian-Antarctic rifted margins was sufficient to form magnetic anomalies that can be used as isochrons despite their formation in lithosphere other than mature, steady-state ocean crust.

1. Introduction

The transition from continental rifting to steady-state ocean spreading is generally characterized by two contrasting end-member models of rifting, corresponding to a magma-poor system with exhumation of subcontinental mantle (Iberia-Newfoundland and Jurassic Western Tethys, e.g., Manatschal, 2004; Whitmarsh et al., 2001), a magma-rich model characterized by a rapid transition from rifting to ocean spreading and extensive magmatism (e.g., South Atlantic; Franke, 2013) with an intermediate model characterized by the rapid production of MORB magmatism during crustal extension (e.g., South China Sea; Larsen et al., 2018).

The Australian-Antarctic conjugate margins represent a locality where the transition from rifting to spreading has been characterized as a magma-poor system (e.g., Gillard et al., 2015; Sayers et al., 2001, Figure 1). In contrast with the Iberia-Newfoundland conjugate margins, the Australian-Antarctic margins lack drill sites, with the result that the width and nature of the ocean-continent transition (OCT) zone is poorly characterized (e.g., Beslier et al., 2004; Nicholls et al., 1981; Niida & Yuasa, 1995). Consequently, two end-member hypotheses have proposed that the OCT is either (i) composed of a wide domain of highly stretched continental crust interspersed with magmatic intrusions and only minor exhumed mantle (e.g., Colwell et al., 2006; Sayers et al., 2001) or (ii) a wide domain of exhumed subcontinental mantle followed by non-steady-state proto-oceanic lithosphere (e.g., Beslier et al., 2004; Gillard et al., 2015).

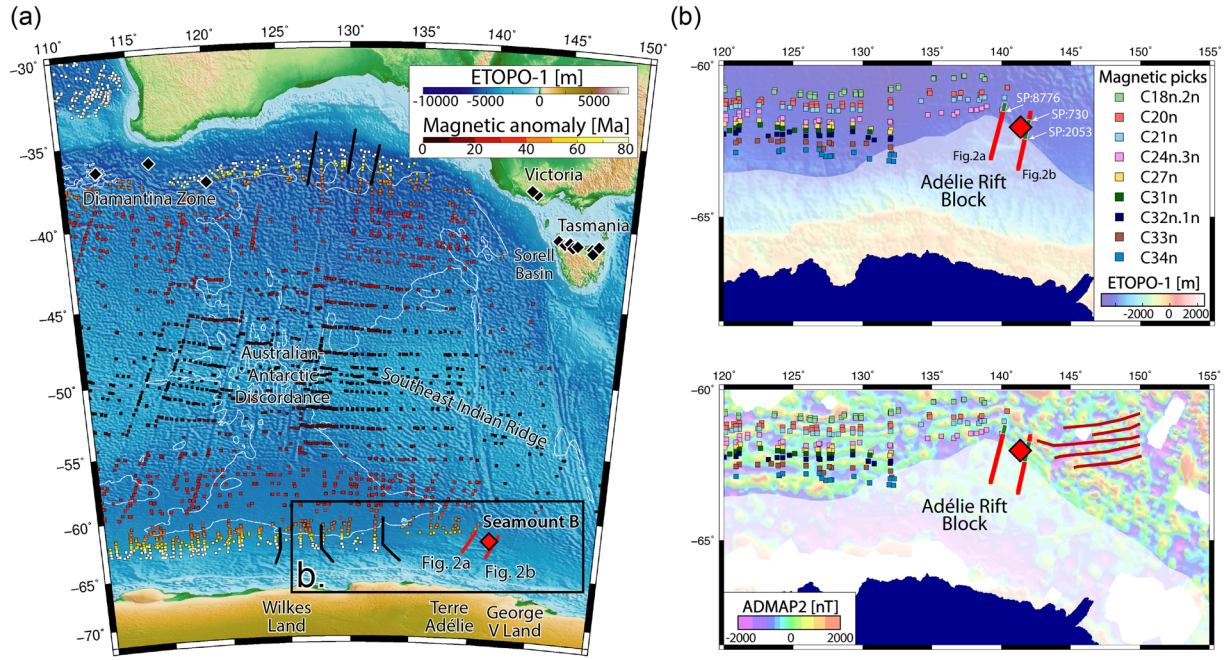

Figure 1. (a) Overview of the Australian-Antarctic margins, using a regional 1-min gravity-derived bathymetric map (ETOPO-1; Amante & Eakins, 2009) and interpreted magnetic anomalies (after Seton et al., 2014). Seamount B dredging locations are shown (red diamond) as well as locations for the Tasmanian, Victorian, and Diamantina zone samples (black diamonds) which are included in this study. Locations of seismic reflection profiles used in this study (red lines) and profiles presented in Gillard et al. (2015, 2016, black lines) are shown. The thin white line defines the Australian-Antarctic Discordance (Whittaker et al., 2010). (b) A detailed view of Seamount B location (red diamond), seismic profiles with shot points (red lines), and the Adélie Rift Block (white shade) is shown, using ETOPO-1 (top) and the Antarctic magnetic anomaly map (bottom, ADMAP2, Golynsky et al., 2018). The zone of exhumed continental mantle determined with the seismic profiles (see Figure 2) is indicated (green line, with shot point [SP] numbers). Note that in the east of Seamount B, additional magnetic lineations have been identified (red lines).

Complicating matters, a symmetrical series of >31,000 km linear magnetic anomalies (C34 to C20) have been interpreted in the OCT zones of the Australian and Antarctic margins (e.g., Tikku & Candes, 1999; Tikku & Cande, 2000; Whittaker et al., 2007; Figure 1). A petrological characterization of the OCT is crucial in order to describe initial magnetic anomalies defining lithospheric breakup and the formation of steady-state oceanic lithosphere (e.g., Matthews & Bath, 1967; Pitman & Heirtzler, 1966; Vine & Matthews, 1963; Williams et al., 2019). The complexity of OCTs implies that defining the first magnetic anomaly related to steady-state oceanic accretion is controversial (e.g., Gillard et al., 2015; Nirrengarten et al., 2018). This includes the magnetic anomalies of the early rift to drift transition along the OCT of the Australian-Antarctic margin (magnetic anomalies C34n and C33n; e.g., Gillard et al., 2015; Tikku & Direen, 2008; Whittaker et al., 2007). In this particular case, the interpretation of these magnetic anomalies as "true" isochrons has been interpreted to imply the onset of steady-state oceanic lithosphere or formed via protracted magmatism and serpentinization during rifting and hyperextension and therefore not "true" isochrons. However, the conflation of linear magnetic anomalies and the production of steady-state oceanic lithosphere are perhaps misleading, given the observation of exhumed lithosphere with linear magnetic anomalies via thin and sparse volcanism at the Southwest Indian Ridge (SWIR; Bronner et al., 2014). Thus, constraining the petrological and structural characteristics of the basement along OCTs is crucial.

We combine multichannel seismic reflection data along Terre Adélie, East Antarctica, in order to define the architecture of the OCT and domains of exhumed mantle with new petrological results from ultramafic rocks dredged from a bathymetric high along the Antarctic margin (Seamount B, Terre Adélie; Niida & Yuasa, 1995; Yuasa et al., 1997). We compare them to mantle xenoliths from syn- to post-rift volcanism in southeast Australia and preserved mantle domains emplaced along OCTs from the Western Tethys (Figure 1). We show that the Australia-Antarctic OCT is comprosed of a 50–100 km wide zone of cold, fertile subcontinental mantle and records similar rift-related magmatic processes as subcontinental mantle domains exhumed along other OCTs and (ultra-) slow spreading systems. This combined geophysical and

petrological study highlights the importance of exhumed mantle domains along present-day ultra-slow spreading OCTs, which were previously uncovered only along the Iberia-Newfoundland rifted margins.

2. Background

2.1. The Australian-Antarctic Rift System

Timing and mechanisms for lithospheric thinning and breakup between Southern Australia and conjugate East Antarctica are controversial (c.f. Eagles, 2019; Williams et al., 2019). The timing of transition from continental rifting to ocean spreading has been proposed to occur between the Late Jurassic to Early Cenozoic (e.g., Jacob & Dyment, 2014; Whittaker et al., 2007, 2013; White et al., 2013; Williams et al., 2011, 2012). Initially, the interpretation of linear magnetic anomalies was used to support the initiation of seafloor spreading in the Eocene (Chron18; Le Pichon & Heirtzler, 1968), an age later revised to Chron22 (ca. 49 Ma), Chron34 (83.5 Ma), or 90–100 Ma (Cande & Mutter, 1982; Veevers, 1986; Weissel & Hayes, 1972), with a NNE–SSW migration of rifting between 160 and 95 Ma (e.g., Powell et al., 1988). Alternatively, Gillard et al. (2015) proposed that large domains of exhumed subcontinental mantle occur along the margins, implying that the first steady-state oceanic crust formed between 53.3 and 43.8 Ma (Chron 24o to 20o). However, the sparse sampled basement material along the Australian-Antarctic margins leaves the nature and width of OCTs ambiguous. Interpretations of geophysical data suggest up to 150 km of discrepancy when defining the initiation of unequivocal oceanic crust (e.g., Close et al., 2009; Colwell et al., 2006; Gillard et al., 2015; Leitchenkov et al., 2007). This leads to conflicting interpretations regarding the nature of magnetic anomalies, whether they can be used as isochrons for plate tectonic reconstructions, and the timing of the rift to drift transition (c.f. Williams et al., 2019; Figure 1).

The complexity of the Australian-Antarctic rift system is further compounded by the Australian-Antarctic Discordance (Figure 1), an unusually deep section of the global mid-ocean ridge system (e.g., Veevers, 1982) coinciding with cooler and/or depleted mantle conditions (Forsyth et al., 1987), chaotic bathymetry, and low magma supply rates (e.g., Christie et al., 1998). This feature has been interpreted either as a zone of downward convecting mantle at the boundary between a Pacific- and Indian-type mantle domain (e.g., Holmes et al., 2010; Veevers, 1982), restricted asthenospheric mantle flow as a result of adjacent thick subcontinental lithosphere and moderate ocean-spreading rates (Buck et al., 2009), or alternatively as resulting from cool depleted mantle domains related to the foundering of the ancient Gondwanaland subducting slab (e.g., Gurnis & Muller, 2003).

2.2. Geological Samples and Constraints Along the Australian-Antarctic Margins

Mantle rocks have been sporadically dredged along the Australian (Beslier et al., 2004; Nicholls et al., 1981) and Antarctic (e.g., Niida & Yuasa, 1995) margins. However, the overall abundance and distribution of mantle rocks along the Australian-Antarctic OCT and their geodynamic relevance has been difficult to assess. In part, this is related to the dynamics of rifting which are likely to vary along the Australian-Antarctic margins (e.g., Direen et al., 2013). Moreover, most parts of the Australian-Antarctic basin are either unusually deep (Australia-Antarctic Discordance; Figure 1) or covered by thick sequences of syn- to post-rift sediments, in particular along the Antarctic margin (e.g., Whittaker et al., 2013), leading to challenges in targeting basement lithologies for dredging and International Ocean Discovery Program (IODP) drilling expeditions.

2.2.1. Seamount B, Antarctica

The (ultra-) slow Australian-Antarctic oblique rift system along the Terre Adélie/George V Land and Sorell Basin, west of Tasmania (Figure 1), provides opportunities to constrain the magmatic and tectonic processes occurring during the final stage of continental breakup of Gondwana between ca. 145 and 35 Ma (e.g., Cande & Mutter, 1982; Stagg & Reading, 2007; Totterdell et al., 2000; Whittaker et al., 2007). This eastern most part of the Australia-Antarctic rift system is a magma-poor oblique rift system with breakup proposed to have occurred in the Maastrichtian (e.g., Direen et al., 2011, 2013; Lavin, 1997; Stagg & Reading, 2007). Japanese dredging expeditions (TH91, TH95; Tanahashi et al., 1997; Yuasa et al., 1997) targeted the oceanic basement along this oblique rift system about 500 km offshore Terre Adélie and George V Land, East Antarctica. These expeditions dredged several seamounts, including Seamount B, a bathymetric feature elevated about 1,000 m above the surrounding seafloor (Site D1201; Niida & Yuasa, 1995; Yuasa et al., 1997) (Figure 1). Preliminary results on several Seamount B samples were published in Yuasa et al. (1997) and Niida and Yuasa (1995), indicating that the majority of dredged samples were variably serpentinized

ultramafic rocks, dominated by fertile lherzolites and pyroxenites. No volcanic rocks were dredged during this expedition, and dredged metamorphic rocks of unknown origin were interpreted as rafted sea-ice debris (Yuasa et al., 1997). The combination of a free-air gravity anomaly at Seamount B, coupled to the lack of dredged volcanic rocks, suggests that Seamount B represents a bathymetric high dominated by unaltered ultramafic rocks (Yuasa et al., 1997). Dredging of bathymetric highs alongside Seamount B did not recover mantle rocks but fragments of continental crust (granite, gneiss, and diorite) (Tanahashi et al., 1997), implying a complex geological environment with a close spatial associated of bathymetric highs dominated by mantle rocks and continental fragments.

2.2.2. Tasmania and Victoria

Mantle fragments or xenoliths sampled from volcanic eruptions (e.g., Nickel & Green, 1984) are a key tool enabling the study of the subcontinental mantle below the continental crust. The mantle xenoliths along the Australian southern margin in Tasmania and Victoria (Beyer, 2002; Frey & Green, 1974; Nickel & Green, 1984; Norman, 1998) are related to volcanism in the Paleocene-Miocene (Tasmania, Beyer, 2002) to Holocene (Southern Victoria, Norman, 1998; Figure 1). These xenoliths range from fertile, amphibole (±phlogopite)-bearing lherzolites to depleted harzburgites with mineral composition and abundances controlled by partial melting and refertilization events (e.g., Beyer, 2002). Overall, these xenoliths indicate the sampling of compositionally heterogeneous, yet generally fertile, cold (<950°C) subcontinental lithosphere along the Australian margin during syn- to post-rifting volcanism.

2.2.3. Diamantina Zone, Western Australia

In 1977 and 1998, variably serpentinized spinel ± plagioclase-peridotites and pyroxenites were dredged in the Diamantina Zone, along the southwestern Australian margin (Beslier et al., 2004; Nicholls et al., 1981; —survey MD110; Figure 1). Although published data from these rocks are sparse (Chatin et al., 1998; Nicholls et al., 1981), these dredging expeditions indicate that subcontinental mantle rocks are exhumed along the western part of the southern Australian margin. The low equilibrium temperatures of these peridotites (T° of 900°C to 1060°C, Nicholls et al., 1981) and fertile compositions combined with spatially associated alkaline magmatism unlike MORB magmatism formed at an oceanic spreading center led Chatin et al. (1998) and Beslier et al. (2004) to suggest that these mantle rocks were emplaced at the ocean floor following continental rifting.

2.3. Magmatic Constraints From Ophiolites and OCTs

Peridotite massifs preserved in orogenic belts (e.g., Bodinier & Godard, 2003; Menzies & Dupuy, 1991) have been used as to constrain magmatic processes occurring in the mantle, including the Lizard (e.g., Green, 1964), Tinaquillo (e.g., Green, 1963), and Ronda (e.g., Masaaki, 1980) massifs, although the origins of these divers peridotite massifs have been debated (c.f. Bodinier & Godard, 2003). In several cases (e.g., Green, 1963, 1964), distinctive peridotites with coarse-grained lherzolite to harzburgite with high-alumina orthopyroxene, clinopyroxene, and spinel are variably overprinted by penetrative foliation and local mylonitization. Remnant pyroxenes porphyroclasts show low-alumina rims matching the compositions of fine-grained, recrystallized matrix mineral and orthopyroxene porphyroclasts show exsolved clinopyroxene lamellae, indicative of decreasing P-T conditions (between 1.5 and 0.5 Gpa). The overprinting of a previous paragenesis can be further recorded by spinel rimmed by plagioclase as well as with olivine, pyroxenes, and Cr-rich spinel and pargasitic amphibole present as a minor or major phase in the foliated matrix, with the appearance of plagioclase implying low pressures.

More recently, ophiolites and peridotite massifs preserved in orogens have been used as an alternative to shipboard drilling and dredging to constrain mantle processes and the formation of oceanic lithosphere from rifting to spreading (e.g., Anonymous, 1972; Bodinier & Godard, 2003; Decandia & Elter, 1972; Lagabrielle & Cannat, 1990; Le Roux et al., 2007). Indeed, ophiolites from the Jurassic-Cretaceous (ultra-) slow spreading Western Tethys preserved in the Western and Central European Alps have similar characteristics as the Iberia-Newfoundland margins. These characteristics include the abundance of partially serpentinized ultramafic rocks, the lack of a dyke complex, sparse MORB magmatism, and marine sediments overlying mantle rocks (e.g., Lagabrielle et al., 2015; Lagabrielle & Cannat, 1990; Lagabrielle & Lemoine, 1997; Manatschal & Müntener, 2009; Picazo et al., 2016). The association of exhumed mantle rocks with hyperextended continental crust and/or tectonosedimentary breccias with continental material (Florineth & Froitzheim, 1994; Manatschal & Nievergelt, 1997; Müntener et al., 2000) indicate that a majority of these ophiolites likely

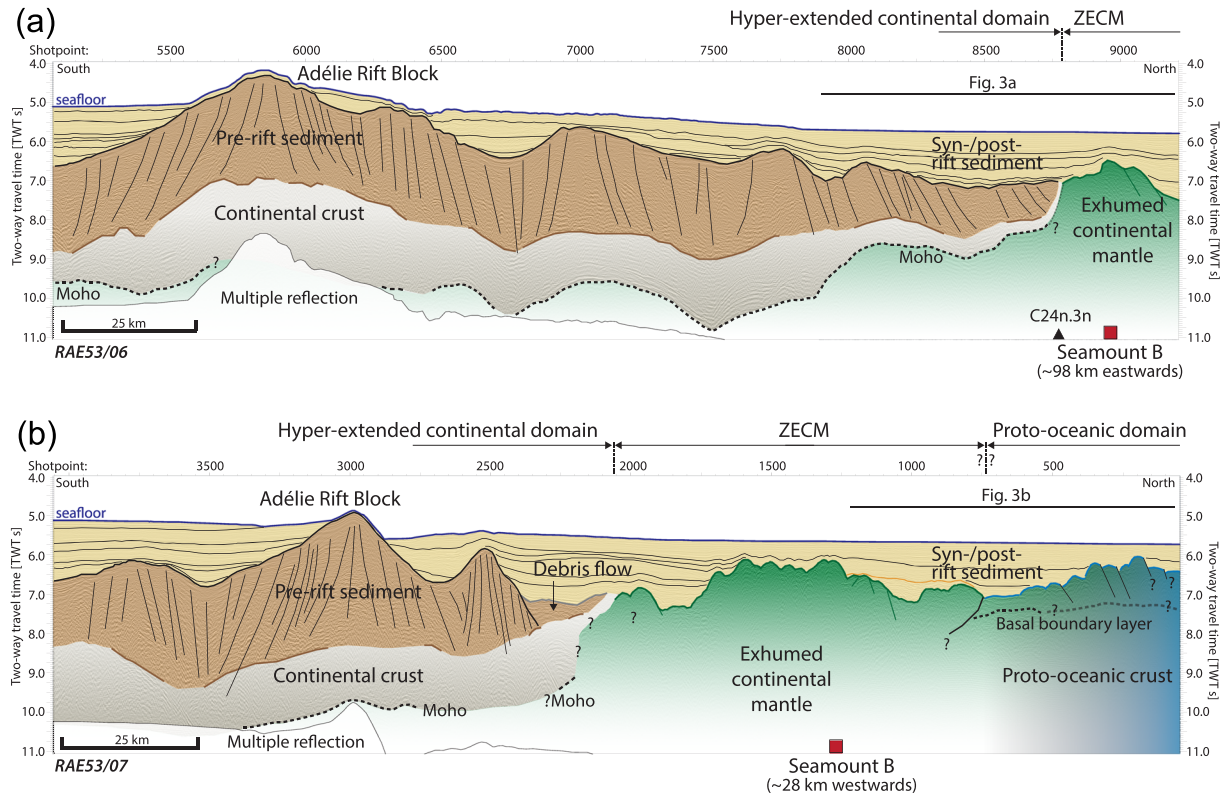

Figure 2. (a, b) Interpreted multichannel seismic reflection transects along each side of Seamount B (location, see Figure 1). The transects are subdivided into three domains: interpreted hyperextended continental domain (a, b), zone of exhumed subcontinental mantle (ZECM; a, b), and proto-oceanic domain (b). Location of Seamount B relative to the profiles is shown (red square). Locations of the detailed zoom-ins of the domains transition zones (Figure 3) are shown (see legend).

represent ultra-slow spreading oceanic domains as well as OCTs, where rifting and thinning out of the continental crust lead to the exhumation of subcontinental lithospheric mantle (e.g., Picazo et al., 2016). Shipboard drilling and dredging along the Iberia-Newfoundland margins expeditions further supported these conceptual models (e.g., Chian et al., 1999; Manatschal, 2004; Whitmarsh et al., 2001).

In terms of magmatism, ophiolites preserved in the Western and Central Alps represent a unique environment allowing mapping of the evolution of petrological characteristics of mantle domains from rifting to ocean spreading (e.g., Picazo et al., 2016). The initial stages of mantle exhumation during rifting along the Western Tethys are accommodated with only sparse to no magmatism. This is likely a consequence of the initial thickness of the cold subcontinental lithospheric mantle leading to the crystallization of melts at higher pressures as well as initial limited mantle melting due to minor lithospheric thinning and asthenospheric upwelling (e.g., Müntener et al., 2010). Thus, an initial "inherited mantle domain" found along hyperextended continental crust is formed of cold (850°C to 950°C), heterogeneous and generally fertile, spinel-bearing subcontinental lithospheric mantle (e.g., Picazo et al., 2016). This inherited mantle domain transitions oceanward into a hybrid "refertilized mantle" domain, dominated by warmer (1000°C to 1100°C) peridotites equilibrated in the plagioclase-stability field and preserving remnant inherited mantle fragments (e.g., Müntener et al., 2010; Picazo et al., 2016; Piccardo et al., 2007). This petrological evolution of mantle rocks along (ultra-) slow OCTs is related to increasing oceanward refertilization of exhumed mantle domains by MORB-type melts during progressive rifting (Picazo et al., 2016). This magmatic evolution can be tracked by the composition of clinopyroxene and spinel as a result of equilibration of MORB melts in the plagioclase-stability field during rifting and transition to (ultra-) slow spreading (Müntener et al., 2010). Thus, mineral compositions in exhumed mantle rocks can be used as fingerprints of magmatic processes occurring prior to and during rifting.

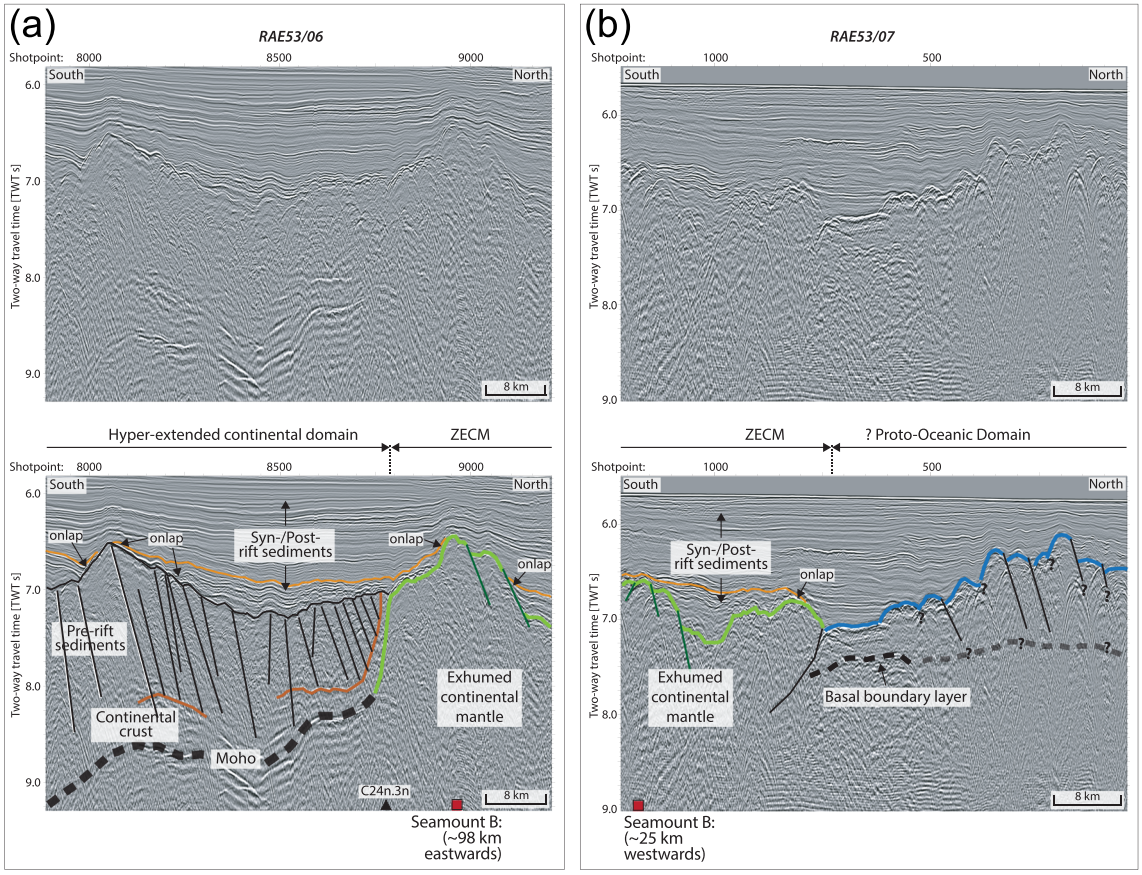

Figure 3. (a, b) Uninterpreted (top) and interpreted (bottom) seismic reflection profiles (location, see Figures 1 and 2) showing the nature and structure of the transitions between (a) hyperextended continental domain and zone of exhumed continental mantle and (b) "proto-oceanic" domain. Location of Seamount B relative to the profiles is shown (red square). Key unconformities/top basement reflections are Moho (thick dashed line), exhumed continental mantle (top, green line), proto-oceanic domain basement (top, blue line; basal reflector, thin dashed line), pre-rift sediments (top, black line), and syn-rift sediments (top, orange line). Faults are shown as thin black lines.

3. Methods and Results

3.1. Seismic Reflection Data

Two multichannel seismic reflection profiles crossing the Antarctic continental margin, that pass closely by each side of Seamount B (Figure 1), have been stratigraphically and structurally analyzed and interpreted (Figures 2 and 3; Russian data set RAE53, source: SCAR's Seismic Data Library System, Wardell et al., 2007). The data were collected in 2008 by the Russian Polar Marine Geosurvey Expedition, using a 352-channel streamer and airguns with a volume of 30–47 L (Leitchenkov et al., 2015). Our seismic interpretation follows the classification and criteria after Gillard et al. (2015, 2016).

3.2. Seismic Stratigraphy

Our seismo-stratigraphic interpretation indicate the presence of three domains along Seamount B, based on their characteristic structural and stratigraphic patterns: hyperextended continental domain, a zone of exhumed continental mantle (ZECM), and a "proto-oceanic" domain that also likely contains exhumed continental mantle with variable amounts of magmatism.

The landward hyperextended continental domain of the Adélie Rift Block shows characteristic closely spaced fault structures, partly domino faults which extend across the entire pre-rift/early rift sedimentary unit (Figures 2 and 3a). "Sag-type" basins are observed within this part of the sedimentary unit, which is a characteristic stratigraphic feature for extended rift sediments.

Table 1
Seamount B Samples, Including Calculated P-T° Conditions

Sample name	Rock type	Primary phases	Microprobe	LA-ICP-MS	Texture	Serpentinization	Pressure (kbar)	$T°_{Ca\text{-}in\text{-}opx}$ (1σ)	$T°_{REE}$ (1σ)
D1201-1	Spl-lherzolite	ol, opx, spl	x	x	Porphyroclastic	High (95%)	—	—	—
D1201-4	Spl-lherzolite	ol, opx, cpx, spl	x		Porphyroclastic	High (75%)	—	896 ± 46	1,050 ± 24
D1302-1	Pl-Spl-lherzolite	ol, opx, cpx, spl, pl, Ti-prg	x	x	Porphyroclastic	Low	—	895 ± 54	—
D1302-2	Pl-Spl-lherzolite	ol, opx, cpx, spl, pl, Ti-prg	x		Porphyroclastic	Low	8.2–9.6	866 ± 50	1,084 ± 22
D1302-6	Pl-Spl-lherzolite	ol, opx, cpx, spl, pl, Ti-prg	x	x	Mylonite	Low	8.2–9.0	885 ± 45	971 ± 22
D1403-6	Pl-Spl-lherzolite	ol, opx, cpx, spl, pl, Ti-prg	x	x	Mylonite	Low	—	864 ± 33	882 ± 39
D1403-13	Pl-Spl-websterite	opx, cpx, spl (hc), pl, Ti-prg	x	x	Mylonite	Low	—	935 ± 42	1,116 ± 29
D1403-14	Pl-Spl-websterite	opx, cpx, spl (hc), pl, Ti-prg	x		Mylonite	Low	—	906 ± 58	—

Note. Due to extensive serpentinization, the presence of plagioclase and amphibole in certain peridotites is unclear. Mineral abbreviations are after Whitney and Evans (2010): ol = olivine; opx = orthopyroxene, cpx = clinopyroxene; spl = spinel; hc = hercynite; pl = plagioclase; prg = pargasite. Note that samples D1201-1 and D1201-4 are highly serpentinized, and their original mineralogy is not fully preserved. Unlike other peridotites however, samples D1201-1 and D1201-4 are characterized by more depleted clinopyroxene composition (Figures 6 and 7) and are plotted separately from amphibole–plagioclase-bearing lherzolites.

In both seismic profiles, a continental dipping, high-amplitude reflector is interpreted as the Moho which is detectable around 10 s two-way travel time (TWT) and rises up to 8 s TWT toward the ocean floor where it disappears (Figures 2 and 3a). Such a sharp shallowing of the Moho is characteristic for domains where exhumation of the subcontinental mantle to the seafloor is observed (e.g., Gillard et al., 2016). Syn-rift sediments onlap onto the exhumed mantle basement, which contains characteristic high-angle fault structures (Figure 3). The imaged basement and overlying sedimentary units along the interpreted zone of exhumed subcontinental mantle are both affected by major deformation structures, which is interpreted as an indicator of exhumed continental mantle, as similar structures are not typically observed in domains of steady-state oceanic crust (e.g., Beslier et al., 1994; Gillard et al., 2015). A prominent debris flow at the oceanward end of the ZECM is detected (Figure 2b), which indicates sediment mass wasting caused by the exhumation of mantle material (after Gillard et al., 2016).

The basement structure changes slightly toward the north; a shallow horizontal high-amplitude reflection pattern is observed which forms a basal boundary layer from which several high-angle faults extend oceanward (Figure 2b and 3b). Such structures have been described as characteristic features for "proto-oceanic" domains (Gillard et al., 2015).

The seismic profiles indicate that the lateral extent of the interpreted ZECM is about 50–100 km wide (Figure 2b). They show a lateral consistency on a regional scale, indicating that Seamount B is located about 30 km oceanward from the hyperextended continental crust into the domain of exhumed subcontinental mantle (Figure 2, Figure 3).

3.3. Petrography

Dredged Seamount B ultramafic rocks comprise lightly to highly serpentinized amphibole-bearing plagioclase-spinel-lherzolites, depleted spinel-lherzolites, and pyroxenites (Table 1). Modal abundances of fresh peridotites indicate mineral abundances between 54–62% olivine, 22–29% orthopyroxene, 6–13% clinopyroxene, <3% Cr-spinel, 0–3.3% plagioclase, and 0–2.7% amphibole (Niida & Yuasa, 1995) whereas pyroxenites have no olivine but contain orthopyroxene (51.9%), clinopyroxene (37.6%), hercynite (6.5%), and minor plagioclase and amphibole (2.8% and 2.1%, respectively) (Niida & Yuasa, 1995). Texturally, these samples grade from porphyroclastic, with large porphyroclasts of variably deformed olivine, orthopyroxene, clinopyroxene to mylonitic with rounded to elongated orthopyroxene (Figure 4). Finer grained interstitial domains are composed of clinopyroxene–plagioclase–olivine ± amphibole rimming porphyroclasts and associated with small embayments along orthopyroxene rims and slight compositional variations in spinel (Figures 4a and 4b). Pyroxenites display large, rounded to strongly elongated porphyroclasts of

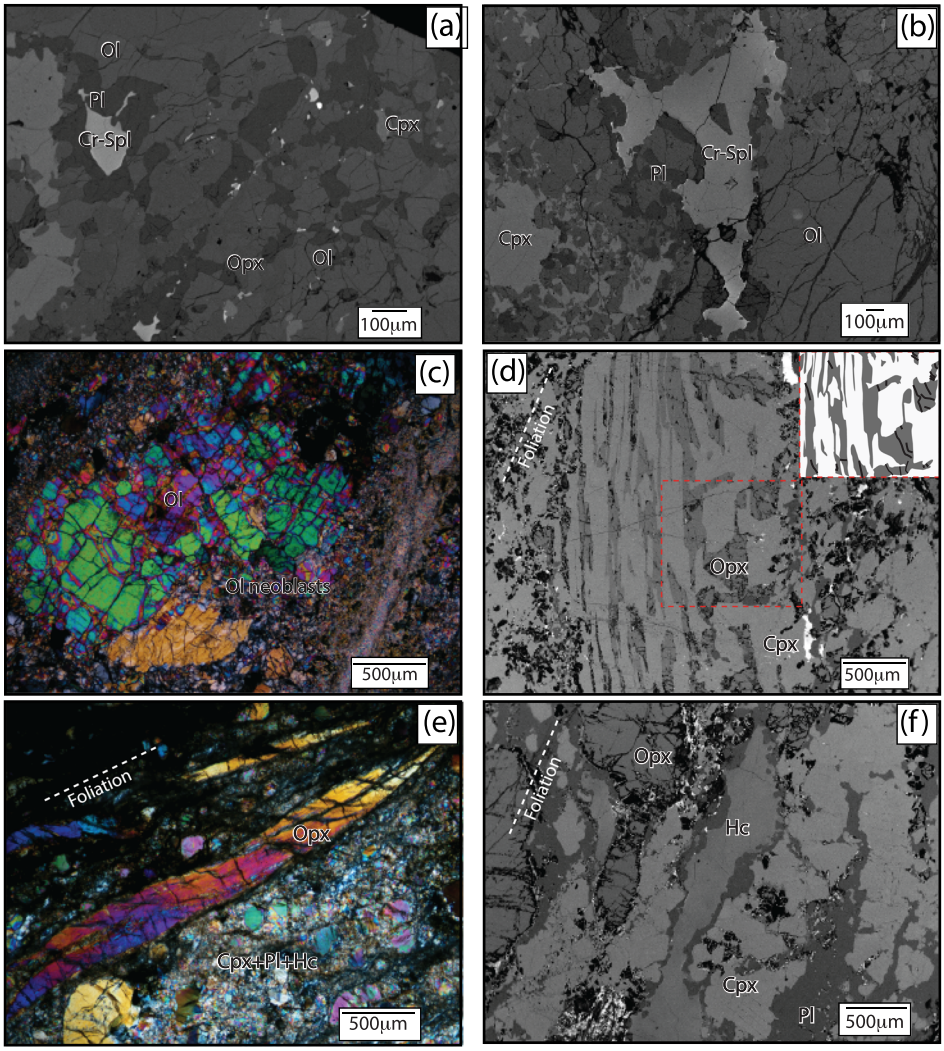

Figure 4. SEM images of textures of Seamount B peridotites and pyroxenites. (a) SEM image of interstitial finer grained assemblage of plagioclase + clinopyroxene + orthopyroxene + olivine + Cr-spinel between large pyroxene in lherzolite sample D1302-1; (b) Cr-spinel rimmed by interstitial plagioclase; note the zonation of Cr-spinel which trends to slightly higher Cr-abundances along certain rims; (c) mylonite texture showing the recrystallization of mantle olivine (peridotite D1403-6); (d) pyroxenite sample D1403-13 showing a large orthopyroxene porphyroclast with extensive clinopyroxene exsolution lamellae; inset in (d) represents a schematic illustration of fractured orthopyroxene with exsolved clinopyroxene; (e) deformed, elongated orthopyroxene (aspect ratio of ~10:1) within a finer grained assemblage of clinopyroxene + plagioclase + hercynite (pyroxenite sample D1403-14); and (f) pyroxenites are dominated by a matrix of finer grained plagioclase + clinopyroxene + hercynite between deformed to rounded orthopyroxene porphyroclasts (pyroxenite sample D1403-13).

orthopyroxene within a finer grained matrix of clinopyroxene, plagioclase, and hercynite (Figures 4d–4f), with occasional orthopyroxene porphyroclasts showing extensive exsolution lamellae of clinopyroxene (Figure 4d).

3.4. Mineral Chemistry

Measurements of major and minor elements on spinel, olivine, pyroxene, and plagioclase were acquired in the geochemical laboratories at the central science laboratory at the University of Tasmania (Australia) on a Microprobe CamecaSX100 and a JEOL JCMA733 at the Hokkaido University (Japan). Analytical conditions were 15 kV acceleration voltage, 25 nA beam current, and a beam size of 1–5 μ. The standards were bustamite (Mn), hematite (Fe), rutile (Ti), nickel silicide (Ni), clinopyroxene (Si and Ca), San Carlos Olivine USNM111312/444 (Mg), Labradorite USNM115900 (Al), Tiebaghi chromite USNM117075 (Cr), Kakanui

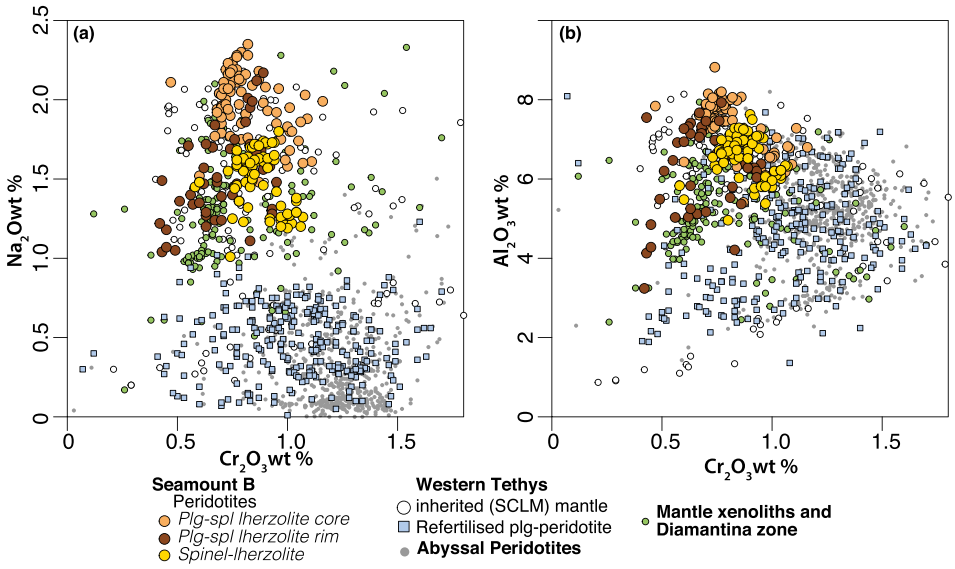

Figure 5. Clinopyroxene composition of Seamount B peridotites. (a) Cr_2O_3 wt% vs. Na_2O wt% and (b) Cr_2O_3 wt% vs. Al_2O_3 wt%. These clinopyroxene are compared to mantle xenoliths from Tasmania and Victoria (Beyer, 2002; Nickel & Green, 1984; Norman, 1998), abyssal peridotites (compilation from Warren, 2016), and Western Tethyan mantle domains subdivided into an "inherited" subcontinental mantle and a "refertilized" mantle domain affected by syn-rift melt percolation (compilation from Picazo et al., 2016). SCLM = subcontinental lithospheric mantle.

anorthoclase USNM133868 (Na), and microcline (K). Counting times were 10 s peak-counting times for Na, Mn, Ti, K ka, Ca ka, and P ka; 30 s peak-counting times for Si and Ni; and 40 s peak-counting times for Al, Fe, Cr, and Mg. Off-peak-counting times were 10 to 20 s on each side of the peak.

In order to determine the pre-exsolution composition of the pyroxenes, "bulk" pyroxene compositions were also acquired as maps on the Cameca SX100 electron microprobe in the central science laboratory at University of Tasmania. Elements were acquired using Kα lines and analyzing crystals LIF for Mn, Fe, Ni, and Cr and LPET for Ti and Ca. The elements Na, Mg, Si, and Al were analyzed on TAP. The calibration standards were San Carlos Olivine (Mg), Plagioclase Lake County (Al), Anorthoclase Kakanui (Na), apecularite (Fe), rutile (Ti), bustamite (Mn), wollastonite (Ca), clinopyroxene (Si), chromite (Cr), and nickel silicide (Ni). The background was corrected using the mean atomic number method (Donovan & Tingle, 1996). Peak times were 400 ms per pixel with a pixel size of 5 × 5 μm and 32 × 32 pixel per map, resulting in a scanned area of 160 × 160 μm on the cores of the pyroxenes. Oxygen was calculated by cation stoichiometry and included in the matrix correction. The matrix correction algorithm utilized was Armstrong/Love Scott (Armstrong, 1988). An average pyroxene composition was calculated for each map and can be found in Supporting Information S1.

Mineral trace element abundances were determined using an Agilent 7500cs quadrupole inductively coupled plasma mass spectrometer (ICP-MS) coupled to a RESOlution HR laser ablation system equipped with a 193 nm Coherent COMPex Pro ArF Excimer Laser and a S155 ablation cell with constant geometry design at the University of Tasmania. A flow of He carrier gas at a rate of 0.35 L/min carried aerosols ablated by the laser out of the chamber to be mixed with Ar gas and carried to the plasma torch. Quantification was performed using NIST612 as the calibration reference material (Jochum & Stoll, 2008) and Ca as the internal standard element. Both BCR-2g and GSD-1g (Jochum & Stoll, 2008) were used as secondary standards for quality monitoring (Supporting Information S1). Both primary and secondary standards were analyzed at the beginning and end of each batch to correct for instrument drift. Data quantification was performed using an in-house data reduction spreadsheet.

3.4.1. Olivine

Olivine in the peridotites has typical mantle value composition, with Mg# (100*Mg/Mg + Fe_{tot}) between 89 and 92 and NiO abundances between 0.32 and 0.45 wt%.

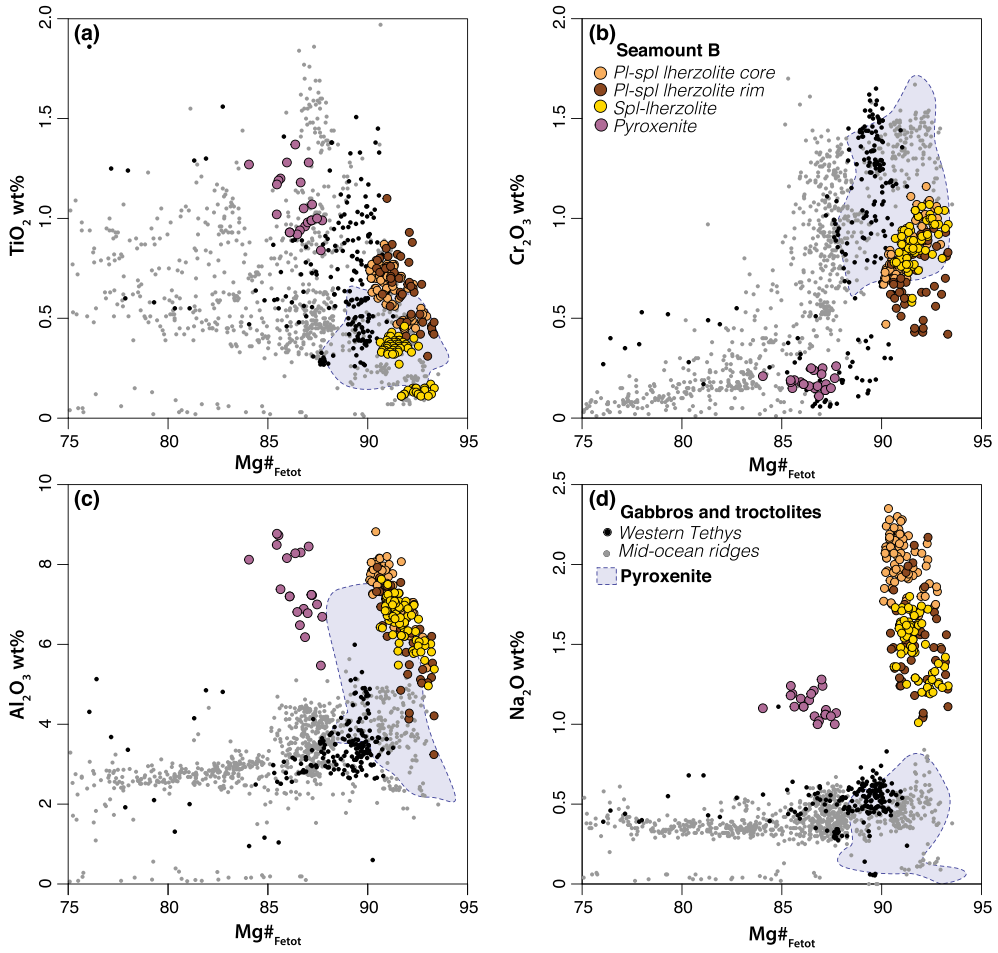

Figure 6. Clinopyroxene composition of Seamount B pyroxenites and peridotites compared to Western Tethys and Mid-Ocean-Ridge gabbros, troctolites, and pyroxenites. (a) $Mg\#_{Fetot}$ vs. TiO_2 wt%; (b) $Mg\#_{Fetot}$ vs. Cr_2O_3 wt%; (c) $Mg\#_{Fetot}$ vs. Al_2O_3 wt%; and (d) $Mg\#_{Fetot}$ vs. Na_2O wt%. Data for the Western Tethys from Rampone et al. (1998), Borghini et al. (2007), Borghini and Rampone (2007), Rampone et al. (2008), Montanini et al. (2008), Renna and Tribuzio (2011), Renna et al. (2016), McCarthy and Müntener (2019), and Basch et al. (2019). Mid-ocean ridge data from Sanfilippo et al. (2013), Dick et al. (2010), Lissenberg and Dick (2008), Suhr et al. (2008) and Leuthold et al. (2018). Pyroxenites from Laukert et al. (2014) and Basch et al. (2019).

3.4.2. Clinopyroxene

Clinopyroxene in lherzolites is found either as large porphyroclasts or as smaller grains (neoblasts) associated with plagioclase and olivine. Clinopyroxene shows elevated Cr_2O_3 abundances (0.45 – 1.16 wt%) and $Mg\#_{Fetot}$ of 90–93.55 (Figure 5). Al_2O_3 and Na_2O abundances decrease with increasing Mg#, from ~8 to 5 wt% and 2.3 to 1 wt%, respectively. Clinopyroxene porphyroclasts show a decrease in Al_2O_3 and Na_2O and increase in Mg# from the core toward the rims, with smaller clinopyroxene having similar composition as clinopyroxene porphyroclast rims (Figures 5 and 6). Clinopyroxene from residual spinel-lherzolites show slightly lower Na_2O, TiO_2, and Al_2O_3 abundances (Figure 5).

Clinopyroxene from pyroxenites show more differentiated compositions compared to clinopyroxene from lherzolites, with $Mg\#_{Fetot}$ between 85.5 and 87.5 and lower abundances in compatible elements such as Cr_2O_3 (<0.25 wt%) and elevated TiO_2 (0.8 – 1.4 wt%) (Figure 6). Clinopyroxene from amphibole-bearing plagioclase-lherzolites have elevated abundances in rare-earth elements (REEs) (Figure 7) with a slight depletion in light-REE for (La_N/Sm_N = 0.23 – 0.4, with N = normalized to chondrite, McDonough & Sun, 1995). The residual spinel-lherzolite shows a distinct REE pattern characterized by a depleted light-REE (La_N/Sm_N = 0.11 – 0.12), consistent with clinopyroxene having lower Na_2O and Al_2O_3

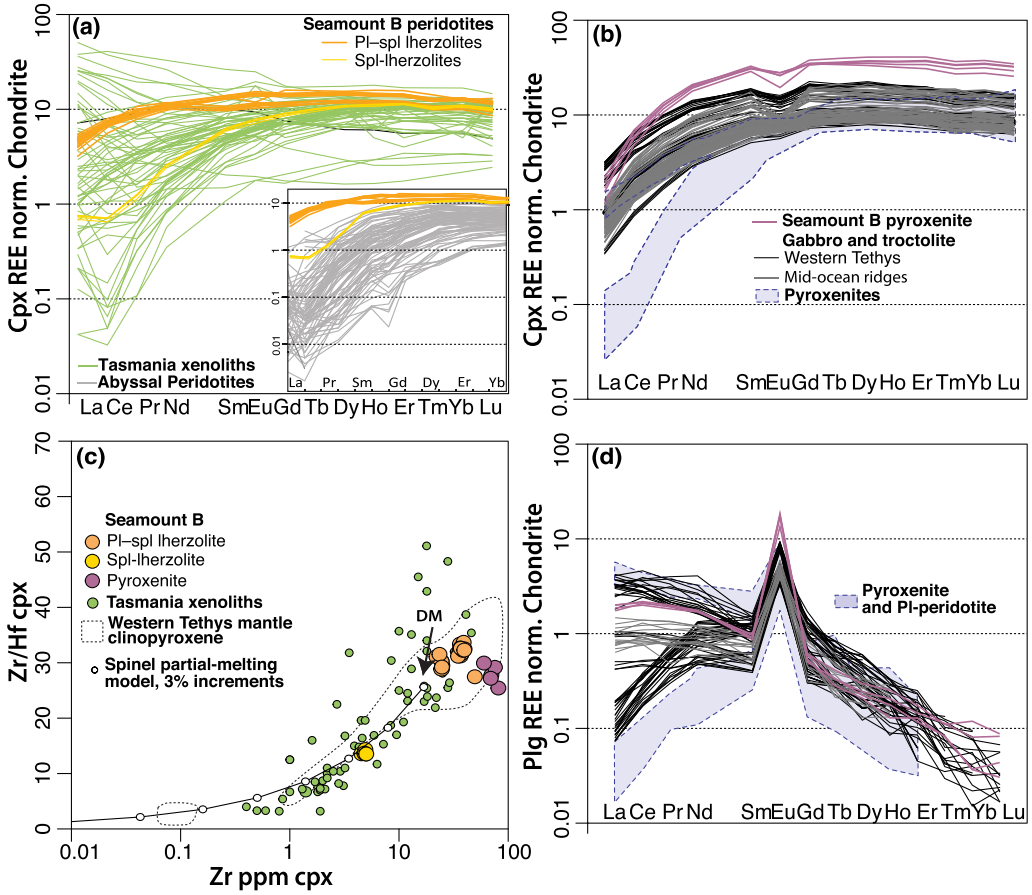

Figure 7. (a) Rare-earth element (REE) of clinopyroxene from Seamount B peridotites compared to clinopyroxene from Tasmania subcontinental mantle xenoliths (Beyer, 2002); inset is the comparison of Seamount B peridotites compared to clinopyroxene from abyssal peridotites (Warren, 2016); (b) REE of clinopyroxene from Seamount B pyroxenites compared to clinopyroxene from gabbros and pyroxenites from (ultra-) slow spreading systems; and (c) Zr/Hf vs. Zr ppm of Seamount B mantle rocks. The black line is a fractional melting model in the spinel stability field starting with a depleted MORB mantle from Workman and Hart (2005) and showing 3% melting increments. Details of partial melting modeling including melting modes and partition coefficients can be found in McCarthy and Müntener (2015, 2019). The spinel-lherzolite sample can be explained by ~5% melting. Subcontinental mantle xenoliths are from Beyer (2002), and the field of Western Tethys mantle clinopyroxene is compiled from McCarthy and Müntener (2019); (d) REE of plagioclase from pyroxenites compared to plagioclase from gabbros and pyroxenites from (ultra-) slow spreading systems. Plagioclase and clinopyroxene compositions from gabbros and troctolites from the Western Tethys are from Borghini and Rampone (2007), Basch et al. (2018), McCarthy and Müntener (2019), from (ultra-) slow spreading ridges from Leuthold et al. (2018) and Drouin et al. (2009). Plagioclase from plagioclase-peridotites are from Rampone et al. (2008) and Basch et al. (2018). Clinopyroxene and plagioclase from pyroxenites are from Laukert et al. (2014) and Basch, Rampone, Crispini, et al. (2019).

(Figures 5 and 7), coupled to a slight enrichment in La (Figure 7a). The pyroxenites show higher abundances in REE and depletion in europium implying cocrystallization with plagioclase.

3.4.3. Orthopyroxene

Orthopyroxene in lherzolites has Mg# between 89.3 and 91.7 and decreases to 86.3–82.0 in pyroxenites. As with clinopyroxene, orthopyroxene shows decreasing Al_2O_3 toward the rims (6 – 2 wt%) whereas Cr_2O_3 (<0.13 wt%) and TiO_2 (<0.18 wt%) abundances remain low. CaO wt% are low in orthopyroxene, ranging between 0.24 and 0.83 wt%, consistent with the presence of exsolution lamellae of clinopyroxene along orthopyroxene cleavage plans.

3.4.4. Plagioclase

Fresh plagioclase is found in lherzolites and pyroxenites. Plagioclase has andesine composition in lherzolites (An30-An42) and labradorite compositions in pyroxenites (An45-An60). REE patterns in plagioclase from pyroxenites show similar L-REE enrichment as oceanic gabbros and abyssal pyroxenites (Figure 7d). Plagioclase is an interstitial phase found rimming spinel or associated with clinopyroxene ± olivine in

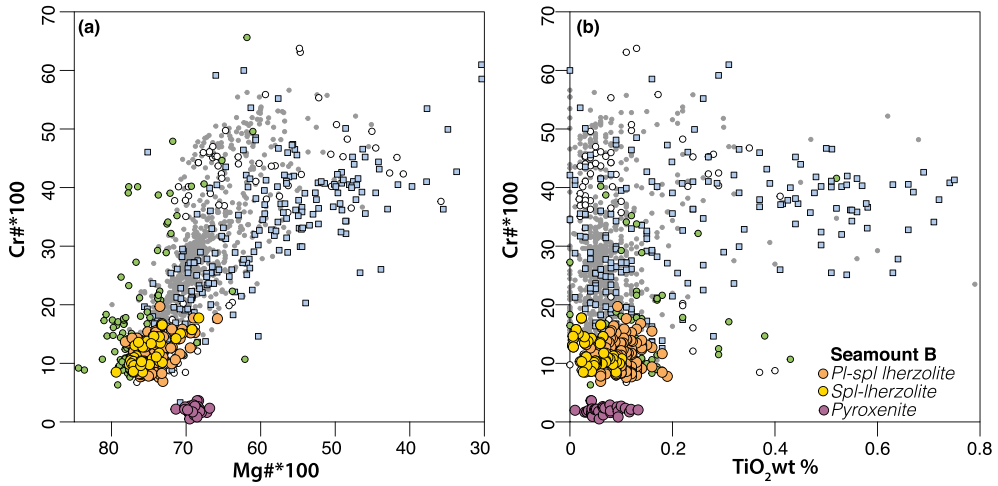

Figure 8. Spinel composition of Seamount B peridotites and pyroxenites compared to western Tethys peridotites and abyssal peridotites. (a) Mg# vs. Cr# and (b) TiO_2 wt% vs. Cr#. Data for comparison are the same as Figure 5.

peridotites (Figures 4a and 4b) and forms the fine-grained matrix with clinopyroxene and hercynite in deformed pyroxenites (Figures 4e and 4f).

3.4.5. Spinel

Cr-spinel is ubiquitous in all lherzolites, homogenous, and characterized by low Cr# (Cr# = Cr/(Cr + Al + Fe^{3+})) ranging between 7 and 20, low TiO_2 abundances (<0.2 wt%), and high Mg# between 68 and 80, with the spinel-lherzolite ranging toward lower TiO_2 abundances (<0.1 wt%) than amphibole-bearing spinel-plagioclase lherzolites (Figure 8). Hercynite in pyroxenites is Cr poor (Cr# < 4) and more enriched in Fe (Mg# = 73 – 66) (Figure 8).

3.4.6. Amphibole

Interstitial amphibole is found in lherzolites and pyroxenites and classified as a pargasite with some high-TiO_2 grains grading toward kaersutite according to the classification of Leake et al. (1997). These amphiboles have high $Mg\#_{Fetot}$ between 86.5 and 90.2 and Cr_2O_3 contents of 0.97 – 1.64 wt%. Na_2O wt% contents remain near constant (3.12 – 3.76 wt%), whereas both TiO_2 and K_2O abundances vary significantly, between 1.7 – 5.5 and 0.02 – 0.41 wt%, respectively.

3.5. Thermometry and Barometry of Seamount B Mantle Rocks

Core to rim zonation of minerals and textural relationships between minerals indicate that bulk equilibrium of the peridotites was not attained. However, pyroxene cores preserve fertile mantle compositions and have been used to calculate equilibrium temperatures (Figure 9a). Equilibrium temperatures for Seamount B mantle rocks were calculated using orthopyroxene major elements and the thermometer of $T°_{Ca\text{-}in\text{-}opx}$ (Brey & Köhler, 1990). As this thermometer is pressure dependent, a pressure of 15 kbar was used is this samples initially equilibrated within the spinel stability field. Average clinopyroxene and orthopyroxene core compositions were used to estimate temperature using the two-pyroxene thermometer (T_{BKN}) of Brey and Köhler (1990) as well as the pyroxene REE thermometer ($T°_{REE}$) of Liang et al. (2013). Equilibrium temperatures range between 892°C (±50°C, 1σ) and 815°C to 860°C for major element thermometers, respectively, whereas T° calculated using REE vary between 882°C and 1116°C (Table 1 and Figure 9). Bulk analysis of orthopyroxene porphyroblast cores give us temperatures of 1091 ± 17 and 1266 ± 54°C (1σ, $T°_{Ca\text{-}in\text{-}opx}$ on samples D1302-1 and D1302-6) as a consequence of the inclusion of clinopyroxene exsolution lamellae and indicative of cooling from high-T° conditions.

The composition of plagioclase is correlated with pressure, with anorthite content of plagioclase decreasing with pressure, and a barometer for plagioclase equilibrium in mantle rocks has been experimentally determined (Borghini et al., 2011; Chalot-Prat et al., 2013; Fumagalli et al., 2017). We have combined interstitial plagioclase and interstitial clinopyroxene pairs as well as rims of clinopyroxene and orthopyroxene porphyroclasts. The application of this barometer using the equations of Fumagalli et al. (2017) in combination with

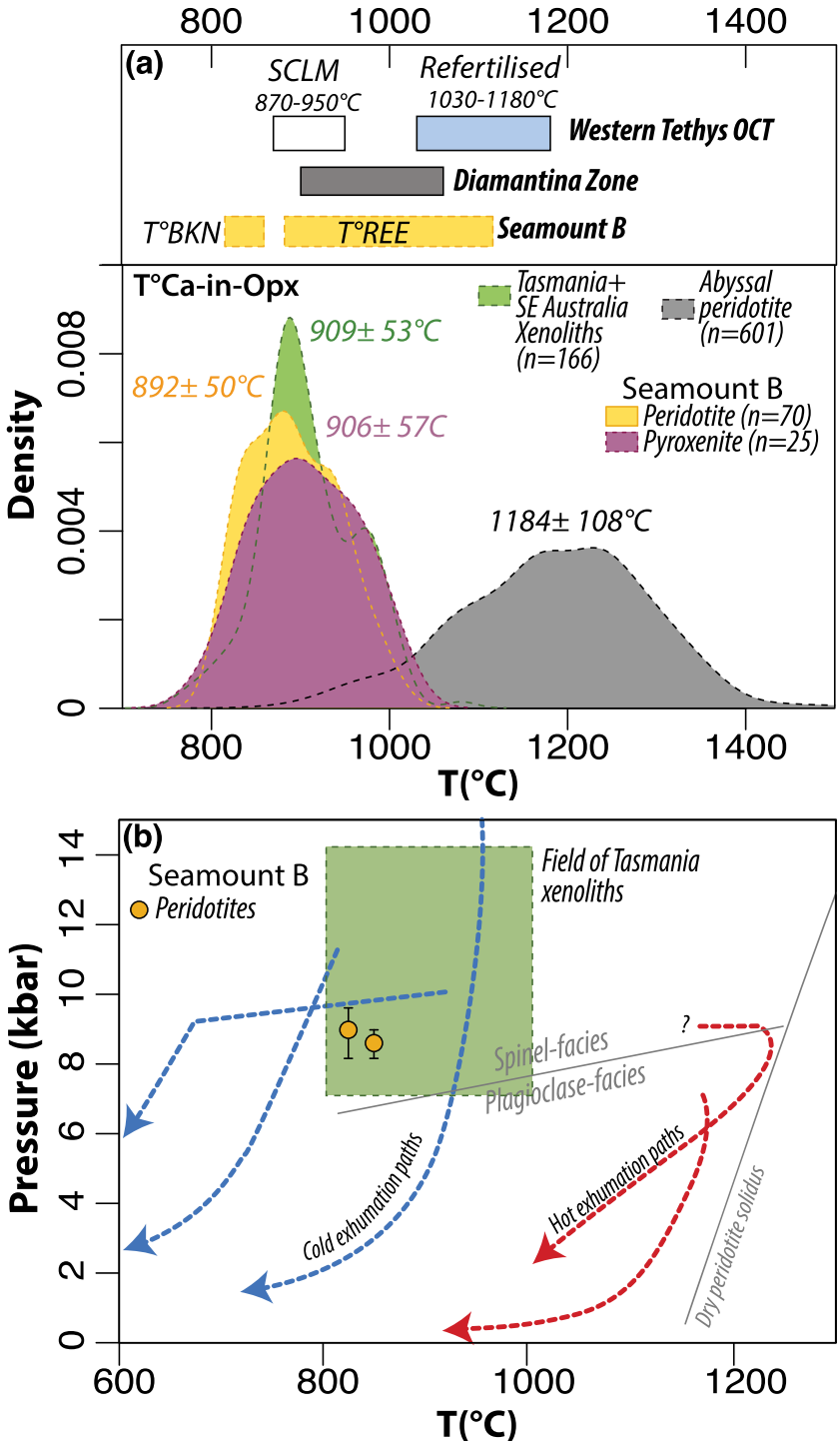

Figure 9. (a) Kernel density distribution of temperatures of peridotites and pyroxenites using $T°_{Ca\text{-}in\text{-}opx}$ (Brey & Köhler, 1990). For comparison, temperatures of exhumed mantle domains along the Western Tethys OCT (European Alps) are plotted (data from Müntener et al., 2010). Note that the increase in temperature from the subcontinental mantle (SCLM) to refertilized mantle domain corresponds to an oceanward evolution of mantle domains as a result of pervasive MORB melt percolation through inherited, cold subcontinental mantle (c.f. Picazo et al., 2016) and (b) pressure estimated for Seamount B plagioclase-bearing spinel-lherzolites. These results are compared to the two distinct P-T paths recorded by exhumed mantle domains at OCTs along the Western Tethys. Cold exhumation paths related to the exhumation of cold SCLM are from Borghini et al. (2011), Montanini et al. (2006), and Müntener et al. (2010). Hot exhumation path related to pervasive and shallow melt percolation during rifting from Piccardo et al. (2009) and Müntener et al. (2010). Estimated temperatures are based on $T°_{Ca\text{-}in\text{-}opx}$ (Brey & Köhler, 1990). Note that the plagioclase-out reaction is a function of bulk composition (e.g., Fumagalli et al., 2017). Error bars for pressure are 1σ.

$T°_{BKN}$ shows high-pressure equilibrium conditions of 8–9 kbar within the upper limit of plagioclase stability at ~860°C to 960°C. These pressure estimates are consistent with the low, and homogenous, anorthite content (An32-An40) of interstitial plagioclase in peridotites (Figure 9). As no olivine was observed in thin section, a prerequisite for the application of this barometer (Fumagalli et al., 2017), we did not calculate pressures for pyroxenites. However, plagioclase in pyroxenites shows overall similar compositions, suggesting similar P-T conditions as the peridotites.

4. Discussion

4.1. Fertile Subcontinental Mantle Along the Australian-Antarctic OCT

The composition of clinopyroxene and Cr-spinel are proxies for partial melting and melt-rock reaction processes (e.g., Dick, 1989; Johnson et al., 1990). Abyssal (oceanic) peridotites show lower Na_2O, and Al_2O_3 and increasing Cr_2O_3 in clinopyroxene and increasing Cr# and decreasing Mg# with low TiO_2 in spinel as a result of adiabatic decompression melting at a mid-ocean ridge (Figures 5 and 8; compilation from Warren, 2016). Seamount B peridotites are distinct from the field of abyssal peridotites, with the cores of clinopyroxene showing Na_2O abundances above 1.5 wt% and Al_2O_3 above 6 wt% whereas spinel Cr# remains <20 and high Mg# (>66) (Figures 5 and 8), implying fertile mantle compositions. A global compilation of trace element abundances in clinopyroxene from abyssal peridotites (Warren, 2016) shows fractionated REE patterns resulting from variable degrees of partial melting (Figure 7a). The trace element abundances of the majority of Seamount B peridotite clinopyroxene indicate only minor partial melting as illustrated in Figures 7a and 7c with lherzolites showing higher trace element abundances (e.g., Zr) than depleted MORB mantle clinopyroxene (Workman & Hart, 2005). Two spinel-peridotites (D1201-1 and D1201-4) have more depleted clinopyroxene compositions than other peridotites, suggesting higher partial melting (Figures 5 and 6). REE patterns of residual spinel-lherzolite D1201-1 indicate a partial melting trend after ~5% melting in the spinel stability field, as illustrated by lower Zr abundances and lower Zr/Hf (Figure 7c) as well as light-REE depleted patterns (Figure 7a).

Calculated T° conditions for Seamount B peridotites from pyroxenes with well-developed exsolved lamellae are below 950°C. Such T° suggest a cold subcontinental mantle origin (Figure 9) whereas the higher temperatures calculated using trace element abundances between orthopyroxene and clinopyroxene ($T°_{REE}$, Figure 9) are consistent with slow cooling rates generally characteristic of subcontinental mantle peridotites (e.g., Dygert & Liang, 2015). In addition, Seamount B peridotites share petrological characteristics similar to subcontinental mantle xenoliths sampled along the Australian margin during syn- to post-rift volcanism (Figure 1a; Nickel & Green, 1984, Norman, 1998, Beyer, 2002). These include similar overlapping pressure-temperature conditions unlike those of abyssal peridotites (Figure 9). Clinopyroxene REE patterns from xenoliths reflect heterogeneous subcontinental mantle lithosphere underneath Tasmania which was affected by variable degrees of partial melting as well as local enrichment in light-REE patterns ascribed to fluid/melt-rock interaction (e.g., Beyer, 2002). REE patterns and Zr abundances of Seamount B clinopyroxene show a distinct overlap with fertile Tasmania xenoliths (Figures 7a and 7c). This is also consistent with overlapping elevated Na_2O and Al_2O_3 abundances of clinopyroxene and lower Cr# and higher Mg# in spinel between Seamount B and xenoliths from the Australian margin (Figures 5 and 8). In addition, positive La_N/Ce_N in depleted spinel-peridotites suggests cryptic infiltration of melt, enriching light-REE elements (Figure 7a) following partial melting, which is a common observation in subcontinental lithosphere below Tasmania (e.g., Beyer, 2002) (Figure 7a). Additionally, the presence of pargasites in these peridotites is indicative of local percolation of melt, or alternatively, minor amounts of fluids through these peridotites, and is a ubiquitous phase in subcontinental lithosphere and in plagioclase-peridotites having been affected by melt-rock interaction (e.g., Frey & Green, 1974; Kaczmarek & Müntener, 2008; Müntener et al., 2010; Vannucci et al., 1995) and represents a late phase crystallizing at temperatures below 1050°C (Niida & Green, 1999).

The combination of cold recorded temperatures, variably fertile mantle compositions and lower degrees of partial melting than is typical for abyssal peridotites (Figures 5, 7a, and 9), therefore suggests that Seamount B represents heterogeneous subcontinental lithosphere variably affected by small amounts of partial melting and local overprint by minor amounts of fluids or melts, as originally proposed by Niida and Yuasa (1995).

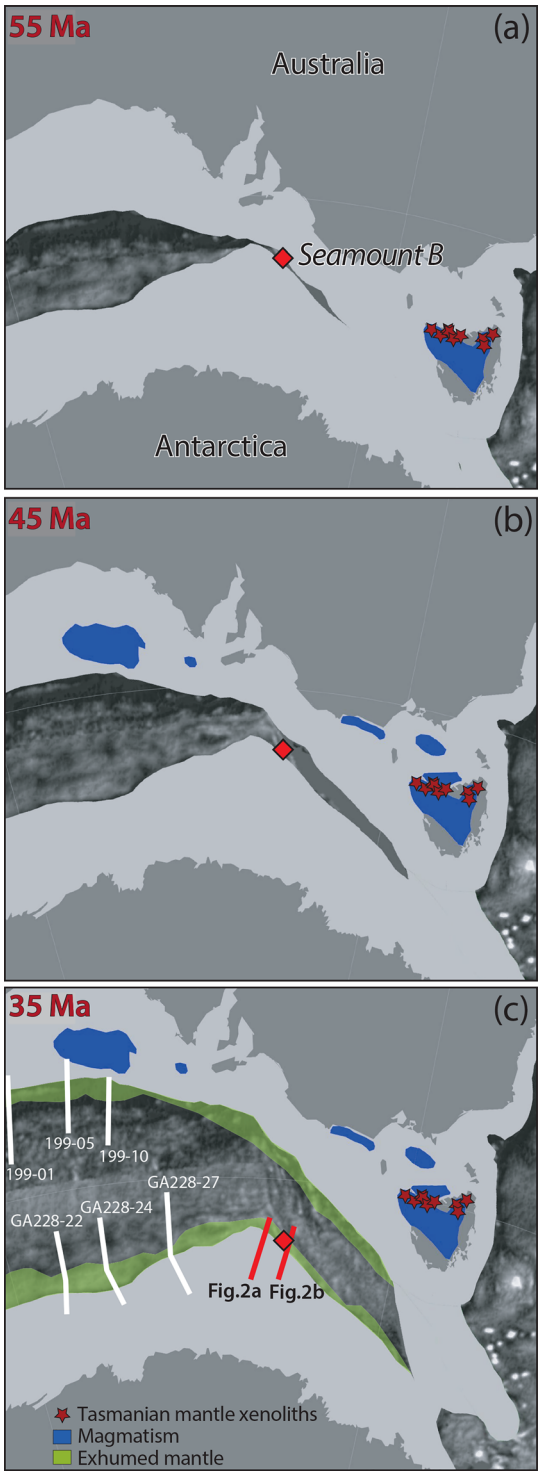

Figure 10. (a–c) Plate tectonic reconstructions showing rifting phase between 55 and 35 Ma (using the plate model of Whittaker et al., 2013), with reconstructed location of Seamount B (red diamond), seismic reflection profiles used in this study (red lines) and profiles presented in Gillard et al. (2015, 2016, white lines). Local magmatism along the Australian-Antarctic margins (blue regions) and Tasmanian mantle xenoliths (Beyer, 2002; red stars) are presented. Interpreted domain of exhumed mantle along the Australian-Antarctic OCT (green regions, for simplicity only drawn in c) are based on data from Seamount B and interpretations from Gillard et al. (2015).

4.2. High-Pressure Melt Impregnation

Plate reconstructions of the rift-to drift transition between 55 and 35 Ma along the eastern section of Australian-Antarctic margins indicate an oblique opening of the Australian-Antarctic Basin along Tasmania (Stagg & Reading, 2007; Figure 10). Such a geometry suggests that the exhumation of Seamount B along the Antarctic OCT (Figures 2, 3, and 10) occurred about 600 km northwest of Tasmania along the Victoria margin. Thus, this indicates that two distinct mechanisms, syn- to post-rift volcanism and (ultra-) slow rifting, were tapping a similar domain of fertile subcontinental mantle with overlapping thermal and petrological characteristics beneath a broad area of the Australian-Antarctic rift system. However, although Seamount B reflects the exhumation of inherited subcontinental mantle to the seafloor, these mantle rocks were likely overprinted by melt impregnation and deformation during exhumation along the OCT.

Plagioclase is a ubiquitous low-pressure aluminum-bearing phase in both abyssal peridotites and in OCTs (e.g., Green, 1964, Dick, 1989, Müntener et al., 2004) and can either form (i) through a subsolidus reaction as a consequence of passive exhumation of mantle to the seafloor: cpx + opx + spl = ol + pl (e.g., Herzberg, 1978; Presnall, 1976; Rampone et al., 1993), or (ii) through percolation of MORB melt as porous flow in mantle rocks along a thermal boundary layer (Dick, 1989; Elthon, 1992; Müntener et al., 2010; Müntener & Piccardo, 2003).

The low temperatures of Seamount B plagioclase-peridotites (Figure 9) unlike other examples of refertilized plagioclase-peridotites (Müntener et al., 2010) as well as the lack of clinopyroxene (Figure 4) and spinel (Figure 8) compositions indicating melt-impregnation events suggest that plagioclase has a metamorphic origin. As such, small core-rim zonation patterns in pyroxene (Figure 5) might well reflect a failure to reach equilibrium during subsolidus decompression. Alternatively, the lack of textural evidence of plagioclase–olivine symplectites recording a metamorphic breakdown of spinel during decompression as well as the presence of interstitial plagioclase rimming spinel and cocrystallization with clinopyroxene (Figures 4a and 4b) suggests a magmatic origin for plagioclase. In addition, subtle core to rim zoning patterns in clinopyroxene (Figure 5) and spinel (Figure 4b), as well as a lack of textural equilibrium in peridotites, could also be indicative of a local refertilization event in the plagioclase-stability field. Indeed, clinopyroxene rims and finer grained clinopyroxene associated with plagioclase have lower Al_2O_3 and Na_2O abundances than clinopyroxene cores, consistent with equilibration of clinopyroxene with plagioclase by percolating MORB melts (e.g., Müntener et al., 2010).

Seamount B pyroxenites show mylonite textures with rounded to strongly elongated porphyroclasts of orthopyroxene rimmed by neoblasts of clinopyroxene + plagioclase and lack olivine (Figures 4d–4f). These pyroxenites do not show any textural evidence of preexisting garnet, a phase generally present in high-pressure pyroxenites in subcontinental lithospheric mantle (e.g., Downes, 2007). Such textural evidence would include the development of symplectites as a consequence of the destabilization of garnet during decompression (e.g., Montanini et al., 2006; Müntener et al., 2010). In terms of mineral composition, the pyroxenites have aluminum-rich spinel (hercynite) (>60 wt% Al_2O_3) unlike spinel from mantle rocks (e.g., Figure 8) as well as clinopyroxene with lower $Mg\#_{Fetot}$ (84–88), Cr_2O_3 abundances (<0.26 wt%), and higher TiO_2 abundances (0.83–1.37 wt%). These pyroxenites are more differentiated than pyroxenites found in abyssal peridotites and along OCTs (e.g., Basch, Rampone, Crispini, et al., 2019) and more consistent with clinopyroxene from troctolites and gabbros for mid-ocean ridge settings (e.g., Drouin et al., 2009; Sanfilippo et al., 2013; Suhr et al., 2008). Thus, this suggests that these pyroxenites formed from melts that were not buffered by the host peridotite (e.g., Basch, Rampone, Crispini, et al., 2019) and that the evolution of these minerals was in part controlled by crystal fractionation upon cooling in the plagioclase-stability field. Thus, whereas peridotites might record either a metamorphic origin of plagioclase or a diffuse event of melt-percolation buffering the mineral assemblage to mantle values, plagioclase-pyroxenites seem to record an enhanced stage of melt impregnation and differentiation in cold subcontinental lithosphere.

The plagioclase barometer of Fumagalli et al. (2017) indicates that peridotites equilibrated at 8–9 kbar (Figure 9b), with pyroxenites likely indicating similar crystallization pressures. Such pressures are significantly higher than generally recorded during melt percolation in mantle rocks exhumed at the seafloor and within the limits of the upper stability of plagioclase in mantle rocks (e.g., Borghini et al., 2009; Fumagalli et al., 2017). Pressure-dependent solid solutions such as jadeite in clinopyroxene (e.g., Borghini et al., 2009; Villiger et al., 2007) are significantly more elevated than for oceanic gabbros and troctolites

and overlap clinopyroxene from peridotites (Figure 6). This suggest that crystallization of an assemblage of cpx + opx + pl + hc occurred at such high pressures (Figure 9). The lack of erupted volcanic products at Seamount B as well as the evolved composition of these minerals implies that we are not able to fully constrain the source of the ascending melt. In addition, enrichment of mid-REE to heavy-REE and Zr (Figure 7b) in clinopyroxene in these pyroxenites compared to troctolites, gabbros, and abyssal pyroxenites might reflect additional post-cumulus crystallization of trapped melts leading to a significant increase in mid-REE to heavy-REE (e.g., Borghini & Rampone, 2007). Nevertheless, experimental studies on the crystallization of MORB have highlighted how pressure controls the abundance of individual phases and mineral compositions. Whereas low-pressure crystallization will lead to the formation of troctolites (olivine-plagioclase) and gabbros (olivine-plagioclase-clinopyroxene) (e.g., Green & Ringwood, 1967; Grove et al., 1992), high-pressure crystallization of slightly differentiated MORB melts leads to the crystallization of a mineral assemblage of clinopyroxene–orthopyroxene–Al-spinel–plagioclase (at 0.7–1 GPa, Villiger et al., 2007). The low anorthite content of plagioclase (<60An) in these pyroxenites thus reflects both the slightly evolved nature of the melt, the elevated pressure of crystallization, and the lack of H_2O in the melt (e.g., Feig et al., 2006; Husen et al., 2016; Panjasawatwong et al., 1995; Villiger et al., 2007).

The presence of mylonite textures and melt impregnation at Seamount B overprinting the subcontinental lithosphere is not unlike other mantle domains emplaced along OCTs, which can show a juxtaposition between melt impregnation and deformation during mantle exhumation (e.g., Kaczmarek & Müntener, 2008). Indeed, subcontinental lithosphere sampled as xenoliths in southeast Australia show primarily granoblastic to pophyroclastic textures (e.g., Beyer, 2002; Frey & Green, 1974; Nickel & Green, 1984) and do not show any textural evidence of plagioclase-bearing mylonites. However, to the contrary of most OCTs (e.g., Fumagalli et al., 2017), Seamount B records evidence of significantly higher melt impregnation and melt differentiation at pressures ≥8 kbar. As Seamount B is located <50 km from the continental margin, these high pressures likely result from the elevated thickness of the subcontinental lithosphere during the initial stages of rifting, preventing partial melts originating from the upwelling asthenosphere from ascending to shallow depth. Thus, although syn-rift magmatism is likely recorded at Seamount B, this exhumed lithospheric mantle acts as a cold high-pressure "lithospheric sponge" (Müntener et al., 2010) storing ascending MORB-type melts and thereby explaining both the lack of dredged gabbros and lavas at Seamount B and the lack of magnetic anomaly atop Seamount B (Figure 1) or linear magnetic anomalies in the ZECM.

4.3. Cold Exhumation Paths and Similarities With Western Tethys Ophiolites

The characteristics of Seamount B include (i) bathymetric features west of Seamount B of continental origin (e.g., Tanahashi et al., 1997) and seismic transects locating Seamount B 20–50 km distant from hyperextended continental crust (Figure 2); (ii) no evidence of volcanic products nor shallow intrusives; (iii) low equilibrium temperatures (Figure 9); (iv) fertile clinopyroxene and spinel compositions implying limited of partial melting (Figures 5–8); (v) low-temperature decompression paths during rifting (Figure 9); and (vi) high-pressure crystallization of MORB-type melts.

The petrology of Seamount B mantle rocks is consistent with interpretations of seismic lines which indicate that extension during late-stage rifting was accommodated by a broad 50–100 km wide zone of exhumed subcontinental mantle between hyperextended continental crust and a proto-oceanic domain (Figures 2 and 3; e.g., Direen et al., 2011, 2013). Seamount B mantle rocks are therefore similar to inherited mantle domains exhumed along an OCT during the initial stages of mantle exhumation in the Western Tethys (Picazo et al., 2016). In addition, the low equilibrium temperatures of these pyroxenites suggest a protracted history of local melt refertilization at high pressure during the initial stage of rifting followed by conductive cooling, consistent with a prolonged period of rifting and crustal thinning along the Australian-Antarctic margins (e.g., Powell et al., 1988).

The continental margin along Seamount B is itself interpreted as a ~200 km wide rifted continental block (Adélie Rift Block) separated from the Antarctic margin by exhumed subcontinental mantle (e.g., Colwell et al., 2006; Direen et al., 2013). Similar characteristics are interpreted along the western Tethys and Iberia margins, where rifted continent blocks are separated by exhumed subcontinental mantle domains (e.g., Manatschal & Müntener, 2009; Manzotti et al., 2014; Whitmarsh et al., 2001). The width of the Western Tethys, where extension was primarily accommodated by crustal thinning and mantle

exhumation is estimated to have reached a maximum width of ≤700 km (e.g., Manatschal & Müntener, 2009; Vissers et al., 2013), with the main basin floored by exhumed mantle (Piemonte-Liguria basin) estimated to have reached a width of 200–300 km (e.g., Manzotti et al., 2014). In addition, Chenin et al. (2017) compiled and assessed the dimensions and architecture of present-day rifted margins and estimated the width of exhumed mantle domains along such OCTs to 20–110 km (median of 70 km). Thus, present-day examples of OCTs, as well as an estimated width for sections of the Western Tethys, suggest that our seismic interpretation of a 50–100 km wide domain of exhumed subcontinental mantle along the Antarctic rifted margin along the Adélie Rift Block (Figures 2 and 3) are well within the range of exhumed mantle domains of OCTs. This estimated width of exhumed subcontinental mantle is also within the range proposed by Gillard et al. (2015) for the central part of the Australian-Antarctic margins (Figure 10) and estimated by Beslier et al. (2004) along the Diamantina Zone of western Australia.

4.4. Magnetic Anomalies Along the Australian-Antarctic OCT

Seamount B is located within a magnetically quiet zone (e.g., Seton et al., 2014; Figure 1c), approximately 50 km inboard of a (proto-) ocean crust based on our interpretation of seismic reflection and magnetic data (Figures 1 and 2). This is consistent with Seamount B being composed of serpentinized mantle rocks and a lack of volcanic products (Tanahashi et al., 1997), as serpentinized peridotites are unlikely to hold a coherent remnant magnetization capable of producing marine magnetic anomalies (Bronner et al., 2014; Maffione et al., 2014). Based on the case study of an OCT in the Western Tethys, Epin et al. (2019) offer further support that OCTs record a transition from no magmatic addition during the initial stages of mantle exhumation to increasing magmatism (shallow gabbroic intrusions and volcanism) oceanward (Müntener et al., 2010). Thus, evidence of melt impregnation at high pressure at Seamount B likely highlights the presence of melt generation during rifting. Melt generation upon rifting is also consistent with compositionally diverse (olivine melilitite to alkali olivine basalts) and discontinuous volcanism along the conjugate margin to Seamount B during rifting (Figure 10), indicating a variably fertile mantle source at depth (Frey et al., 1978). The gradual thinning of the subcontinental mantle and upwelling asthenosphere would then lead to the emplacement of gabbros at shallow depth and local volcanism further oceanward of Seamount B, coinciding with the appearance of a first (C24n.3n) magnetic anomaly (Figure 1). Additionally, geophysical observations along the Southwestern Indian Ridge (Cannat et al., 2019) indicate that (ultra-) slow spreading systems transition from a nearly amagmatic spreading controlled by low-angle detachment faults and exhumation of oceanic core complexes to more magma-rich segments over less than 30 km. Thus, as a consequence of the thermal state and rheology of the lithosphere (Cannat et al., 2019), melt production might vary significantly along strike, with ascending melts either being erupted along volcanic-rich segments or forming impregnated plagioclase-peridotites along magma-poor segments. In both the Bight Basin and conjugate Wilkes Land margin, linear magnetic anomalies (e.g., Golynsky et al., 2012) extending for >1,000 km are observed across regions which have been interpreted as continental crust, exhumed continental mantle, and "proto-oceanic" crust (e.g., Close et al., 2009; Colwell et al., 2006; Gillard et al., 2015; Leitchenkov et al., 2007). Evidence of magmatism during mantle exhumation along Seamount B thus suggests that many magnetic anomalies, including C34y and C33o, but also extending to C24o and C20y (Tikku & Candes, 1999; Whittaker et al., 2007) might result from sparse volcanic and shallow magmatic additions to the exhumed (subcontinental or oceanic) mantle domain (e.g., Bronner et al., 2014) as a consequence of alternating magmatic and nearly amagmatic segments (e.g., Cannat et al., 2019).

4.5. Elucidating the Nature of Mantle Domains Along the Australia-Antarctic Margins: The Case for Further Shipboard Expeditions

Bathymetric features similar to Seamount B are ubiquitous throughout the Australian-Antarctic margins, and variously interpreted as volcanic edifices, peridotite ridges, or crustal blocks, depending on recovered dredged samples, geophysical properties, and distance to the continental shelf (e.g., Gillard et al., 2015, 2016). The presence of bathymetric features with continental rocks in close proximity to Seamount B (Tanahashi et al., 1997) as well as the segmented architecture of (ultra-) slow spreading lithosphere (Cannat et al., 2019) underscores the structural complexity of (ultra-) slow spreading systems. Therefore, the Australian Southern Ocean represents a unique location where targeting bathymetric features along the Australian and Antarctic OCTs will help resolve magmatic and tectonic controversies and test mechanisms of rifting and spreading along (ultra-) slow spreading systems initially developed along Iberia-Newfoundland OCTs and the Western Tethys. Here we highlight some key petrological and tectonic questions that could be resolved by future IODP drilling expeditions.

Tectonic subsidence curves modeled from industry well site data in sedimentary basins along the Australian OCT record an abnormal lack of subsidence during the early post-rift phase (~85 to ~50 Ma; Brown et al., 2003; Totterdell et al., 2000). Although some minor subsidence during this time period can be observed at the drill sites in the more oceanward sedimentary basins, their rates are much lower than the expected McKenzie (1978) thermal subsidence of extended rift basins. Subsidence of passive margins is expected to occur during the rift to drift transition due to crustal thinning, cooling of the lithosphere, and sedimentary loading (e.g., Bott, 1992). However, the exhumation of cold subcontinental lithosphere to the sea floor coupled with melt impregnation upon exhumation might lead to a retardation of basin subsidence. In the Australian-Antarctic context, this implies mantle exhumation until approximately 50 Ma, consistent with the interpretation of Gillard et al. (2015) for the transition to steady-state oceanic spreading. Western Tethys OCTs indicate that extensive percolation of MORB melt forming plagioclase-peridotites can lead to a storage of 12% of ascending melt (Müntener et al., 2010). Extensive heating of cold subcontinental lithosphere will lead to the formation of more buoyant lithosphere (e.g., Chenin et al., 2017). For example, the western Antarctic rift system is characterized by anomalous high heat flow interpreted as resulting from syn-rift melt percolation leading to the formation of refertilized, plagioclase-peridotites incorporating up to 8% MORB-type melt (e.g., Martin et al., 2014). In addition, numerical modeling simulating hyperextension of subcontinental lithosphere indicates that the transition from spinel-bearing peridotites to plagioclase-bearing peridotites leads to a significant decrease in mantle density, thereby limiting subsidence (Kaus et al., 2005; Minakov & Podladchikov, 2012; Simon & Podladchikov, 2008). Seamount B represents the initial stages of exhumation of inherited, cold subcontinental mantle which might record early stages of high-pressure melt impregnation. Thus, extensive melt percolation is likely to occur oceanward. The Australian-Antarctic OCT therefore represents a unique environment to test whether retardation of basin subsidence might be controlled by the mechanism of extraction (volcanism) or storage ("lithospheric sponge") of MORB melt along an (ultra-) slow spreading system (e.g., Müntener et al., 2010).

Moreover, the low equilibrium T° of these mantle rocks, the fertile nature of Seamount B samples, evidence of melt impregnation, and the lack of dredged MORB volcanism along the Antarctic margin (Yuasa et al., 1997) is consistent with a lack of partial melting of Seamount B mantle rocks upon exhumation. This implies that the partial melting event recorded in the depleted spinel-lherzolites likely reveal "ancient" magmatic processes unrelated to rifting and mantle exhumation (e.g., McCarthy & Müntener, 2015; Rampone et al., 1998). Depleted mantle domains along OCTs and (ultra-) slow spreading localities are interpreted as preserving "ancient" melting events, such as (i) Proterozoic melting events (Macquarie Island, Southern Ocean, Dijkstra et al., 2010), (ii) Permian mantle-derived magmatism (Western Tethys, e.g., McCarthy & Müntener, 2015, 2019), (iii) subarc mantle during Pan-African Orogeny found in the Zabargad ophiolite (Red Sea, Brooker et al., 2004), and (v) subarc mantle along Newfoundland margin (ODP Site 1277; Müntener & Manatschal, 2006) and western Iberia/Morocco margin (volcanic xenoliths; Merle et al., 2012). The presence of a relic subduction zone along eastern Gondwanaland is suggested to be responsible of the formation of the Australian-Antarctic Discordance (Gurnis & Muller, 2003). Seamount B mantle rocks and Tasmanian and Victorian xenoliths indicate the presence of a wide domain of fertile subcontinental mantle along southeast Australia to the east of the Australian-Antarctic Discordance (Figures 5–9). Thus, in accordance with Gurnis and Muller (2003), exhumed mantle domains closer to the Australia-Antarctic Discordance should reflect characteristics of subduction zone processes, such as the more depleted nature of the mantle and fluid/melt-rock reactions as a consequence of (ancient) slab dehydration and/or melting (e.g., Bryant et al., 2007). The Australian-Antarctic spreading system therefore represents a key locality to study the effect of magmatic inheritance and the origin(s) of mantle heterogeneity in (ultra-) slow spreading systems (e.g., McCarthy & Müntener, 2015; Rampone & Hofmann, 2012; Sanfilippo et al., 2019; Warren et al., 2009) by targeting (i) the heterogeneity of abyssal peridotites along the active Southeast Indian Ridge, (ii) the evolution of mantle rocks along the Australia-Antarctic discordance, and (iii) the oceanward compositional evolution of mantle domains at OCTs.

5. Conclusions

We combine multichannel seismic reflection data and petrological measurements of dredged mantle rocks along Terre Adélie (East Antarctica) and show the presence of a 50–100 km wide domain of exhumed mantle which formed along the Terre Adélie/George V Land and Sorell Basin along the Australian-Antarctic rift

system. These mantle rocks represent fertile, cold (900°C) subcontinental mantle exhumed at the ocean floor during rifting. Seamount B mantle rocks show similar petrological characteristics as mantle xenoliths from the Australian margin, indicating that both (ultra-) slow spreading and volcanism sampled similar underlying subcontinental lithosphere. Syn-rift magmatism and melt differentiation are recorded by MORB melt crystallization at ≥8 kbar, leading to formation of plagioclase-pyroxenites. The initial stages of mantle exhumation during rifting likely inhibited volcanism and shallow melt intrusions due to the thickness of the cold subcontinental lithosphere. Thus, evidence of melt percolation at Seamount B suggests that syn-rift magmatism was prevalent, which suggests that magnetic anomalies result from thin, sparse volcanic/magmatic additions to the exhumed mantle domain during lithospheric extension and the transition toward steady-state oceanic lithosphere. Finally, we propose that the magmatic processes recorded during (ultra-) slow spreading along the Australian-Antarctic OCT might represent a recent analogue to Jurassic Western Tethys OCTs and represent a key target for future drilling and dredging expeditions.

Data Availability Statement

The seismic reflection data are freely available through the Seismic Data Library System of SCAR (https://www.scar.org/sdls/), and geochemical analyses of minerals are freely available on the Institute of Marine and Antarctic Sciences (IMAS, University of Tasmania) Metadata Catalogue website (doi: 10.25959/5e6810710ac85). We thank S. Gilbert, J. Thompson, and S. Feig for their help with obtaining geochemical analyses. We are grateful for discussions with O. Müntener and reviews by R. Buck and an anonymous reviewer as well as editorial handling by Whitney Behr which helped clarify the manuscript.

Acknowledgments

A. M. acknowledge the support of Swiss National Science Foundation grant P2LAP2_171819. I. S. was supported under Australian Research Council's Special Research Initiative for Antarctic Gateway Partnership (Project ID SR140300001). J. M. W. acknowledges support from Australian Research Council grant DP180102280. We are also grateful to the support from the SCAR community as well as to Dr. M. Yuasa of the Geological Survey of Japan for having carried out the initial studies on Seamount B.

References

Amante, C., & Eakins, B. W. (2009). ETOPO1 1 arc-minute global relief model: Procedures, data sources and analysis. *NOAA Technical Memorandum NESDIS*, *NGDC-24*, 19.

Anonymous (1972). Penrose field conference on ophiolites. *Geotimes*, *17*, 24–25.

Armstrong, J. T. (1988). *Quantitative analysis of silicates and oxide minerals: Comparison of Monte-Carlo, ZAF and Phi-Rho-Z procedures*, (pp. 239–246). San Francisco, CA: Microbeam Analysis.

Basch, V., Rampone, E., Borghini, G., Ferrando, C., & Zanetti, A. (2019). Origin of pyroxenites in the oceanic mantle and their implications on the reactive percolation of depleted melts. *Contributions to Mineralogy and Petrology*, *174*, 97. https://doi.org/10.1007/s00410-019-1640-0

Basch, V., Rampone, E., Crispini, L., Ferrando, C., Ildefonse, B., & Godard, M. (2018). From mantle peridotites to hybrid troctolites: Textural and chemical evolution during melt-rock interaction history (Mt. Maggiore, Corsica, France). *Lithos*, *323*, 4–23. https://doi.org/10.1016/j.lithos.2018.02.025

Basch, V., Rampone, E., Crispini, L., Ferrando, C., Ildefonse, B., & Godard, M. (2019). Multi-stage reactive formation of troctolites in slow-spreading oceanic lithosphere (Erro–Tobbio, Italy): A combined field and petrochemical study. *Journal of Petrology*, *60*, 873–906. https://doi.org/10.1093/petrology/egz019

Beslier, M. O., Cornen, G., Sawyer, D. S., Whitmarsh, R. B., Klaus, A., Collins, E. S., et al. (1994). Péridotites et gabbros à la transition continent-océan d'une marge passive: Résultats préliminaires du leg ODP 149 dans la Plaine Abyssale Ibérique. *Comptes rendus de l'Académie des sciences*, *Série 2*, 319, 10, (1223–1229). Sciences de la terre et des planètes.

Beslier, M. O., Royer, J. Y., Girardeau, J. A., Hill, P. J., Boeuf, E. R., Buchanan, C. A., et al. (2004). Une large transition continent-océan en pied de marge sud-ouest australienne: premiers résultats de la campagne MARGAU/MD110. *Bulletin Société géologique Francaise*, *175*, 629–641. https://doi.org/10.2113/175.6.629

Beyer, E. E., (2002). Evolution of the lithosphere beneath Tasmania and western Norway. Ph.D. thesis, Macquarie University, Sydney, 336 pp.

Bodinier, J. L., & Godard, M. (2003). Orogenic, ophiolitic, and abyssal peridotites. In R. W. Carlson, H. D. Holland, & K. K. Turekian (Eds.), *Treatise on geochemistry*, (Vol. 2, p. 568). Oxford: Elsevier-Pergamon.https://doi.org/10.1016/B0-08-043751-6/02004-1

Borghini, G., Fumagalli, P., & Rampone, E. (2009). The stability of plagioclase in the upper mantle: Subsolidus experiments on fertile and depleted Lherzolite. *Journal of Petrology*, *51*, 229–254. https://doi.org/10.1093/petrology/egp079

Borghini, G., Fumagalli, P., & Rampone, E. (2011). The geobarometric significance of plagioclase in mantle peridotites: A link between nature and experiments. *Lithos*, *126*, 42–53. https://doi.org/10.1016/j.lithos.2011.05.012

Borghini, G., & Rampone, E. (2007). Postcumulus processes in oceanic-type olivine-rich cumulates: The role of trapped melt crystallization versus melt/rock interaction. *Contributions to Mineralogy and Petrology*, *154*, 619–633. https://doi.org/10.1007/s00410-007-0217-5

Borghini, G., Rampone, E., Crispini, L., De Ferrari, R., & Godard, M. (2007). Origin and emplacement of ultramafic–mafic intrusions in the Erro-Tobbio mantle peridotite (Ligurian Alps, Italy). *Lithos*, *94*, 210–229. https://doi.org/10.1016/j.lithos.2006.06.014

Bott, M. H. P. (1992). Passive margins and their subsidence. *Journal of the Geological Society*, *149*(5), 805–812. https://doi.org/10.1144/gsjgs.149.5.0805

Brey, G. P., & Köhler, T. (1990). Geothermobarometry in four-phase lherzolites II. New thermobarometers, and practical assessment of existing thermobarometers. *Journal of Petrology*, *31*(6), 1353–1378. https://doi.org/10.1093/petrology/31.6.1353

Bronner, A., Sauter, D., Munschy, M., Carlut, J., Searle, R., Cannat, M., & Manatschal, G. (2014). Magnetic signature of large exhumed mantle domains of the Southwest Indian Ridge: Results from a deep-tow geophysical survey over 0 to 11 Ma old seafloor. *Solid Earth Discussions*, *5*, 2449–2482. https://doi.org/10.5194/sed-5-2449-2013

Brooker, R. A., James, R. H., & Blundy, J. D. (2004). Trace elements and Li isotope systematics in Zabargad peridotites: Evidence of ancient subduction processes in the Red Sea mantle. *Chemical Geology*, *212*, 179–204. https://doi.org/10.1016/j.chemgeo.2004.08.007

Brown, B. J., Muller, R. D., Gaina, C., Struckmeyer, H. I. M., Stagg, H. M. J., & Symonds, P. A. (2003). Formation and evolution of Australian passive margins: Implications for locating the boundary between continental and oceanic crust. *Special Papers Geological Society of America*, *372*, 223–244. https://doi.org/10.1130/0-8137-2372-8.223

Bryant, J. A., Yogodzinski, G. M., & Churikova, T. G. (2007). Melt-mantle interactions beneath the Kamchatka arc: Evidence from ultramafic xenoliths from Shiveluch volcano. *Geochemistry, Geophysics, Geosystems*, *8*, Q04007. https://doi.org/10.1029/2006GC001443

Buck, W. R., Small, C., & Ryan, W. B. (2009). Constraints on asthenospheric flow from the depths of oceanic spreading centers: The East Pacific rise and the Australian-Antarctic Discordance. *Geochemistry, Geophysics, Geosystems*, *10*, Q09007. https://doi.org/10.1029/2009GC002373

Cande, S. C., & Mutter, J. C. (1982). A revised identification of the oldest sea-floor spreading anomalies between Australia and Antarctica. *Earth and Planetary Science Letters*, *58*(2), 151–160. https://doi.org/10.1016/0012-821X(82)90190-X

Cannat, M., Sauter, D., Lavier, L., Blickert, M., Momoh, E., & Leroy, S. (2019). On spreading modes and magma supply at slow and ultraslow mid-ocean ridges. *Earth and Planetary Science Letters*, *519*, 223–233. https://doi.org/10.1016/j.epsl.2019.05.012

Chalot-Prat, F., Falloon, T. J., Green, D. H., & Hibberson, W. O. (2013). Melting of plagioclase + spinel lherzolite at low pressure (0.5 GPa): An experimental approach to the evolution of basaltic melt during mantle refertilization at shallow depths. *Lithos*, *172-173*, 61–80. https://doi.org/10.1016/j.lithos.2013.03.012

Chatin, F., Robert, U., Montigny, R., & Whitechurch, H. (1998). La zone Diamantine (océan Indien oriental), témoin de la séparation entre l'Australie et l'Antarctique: arguments pétrologiques et géochimiques. *Comptes Rendus de l'Académie des Sciences - Series IIA - Earth and Planetary Science*, *326*(12), 839–845. https://doi.org/10.1016/S1251-8050(98)80022-0

Chenin, P., Manatschal, G., Picazo, S., Müntener, O., Karner, G., Johnson, C., & Ulrich, M. (2017). Influence of the architecture of magma-poor hyperextended rifted margins on orogens produced by the closure of narrow versus wide oceans. *Geosphere*, *13*, 559–576. https://doi.org/10.1130/GES01363.1

Chian, D., Louden, K. E., Minshull, T. A., & Whitmarsh, R. B. (1999). Deep structure of the ocean-continent transition in the southern Iberia abyssal plain from seismic refraction profiles: Ocean drilling program (legs 149 and 173) transect. *Journal of Geophysical Research*, *104*(B4), 7443–7462. https://doi.org/10.1029/1999JB900004

Christie, D. M., West, B. P., Pyle, D. G., & Hanan, B. B. (1998). Chaotic topography, mantle flow and mantle migration in the Australian–Antarctic discordance. *Nature*, *394*(6694), 637–644. https://doi.org/10.1038/29226

Close, D. I., Watts, A. B., & Stagg, H. M. J. (2009). A marine geophysical study of the Wilkes Land rifted continental margin, Antarctica. *Geophysical Journal International*, *177*, 430–450. https://doi.org/10.1111/j.1365-246X.2008.04066.x

Colwell, J. B., Stagg, H. M. J., Direen, N. G., Bernarde, G., & Borissova, I. (2006). The structure of the continental margin off Wilkes Land and Terre Adelie, East Antarctica. In D. K. Fütterer, et al. (Eds.), *Antarctica: Contributions to Global Earth Sciences*, (pp. 327–340). Berlin: Springer. https://doi.org/10.1007/3-540-32934-X_41

Decandia, F. A., & Elter, P. (1972). La "zona" ofiolitifera del Bracco nel settore compreso fra Levanto e la Val Gravena (Apennino ligure). *Società Geologica Italiana. Bulletin*, *11*, 37–64.

Dick, H. J., Lissenberg, C. J., & Warren, J. M. (2010). Mantle melting, melt transport, and delivery beneath a slow-spreading ridge: The paleo-MAR from 23°15′N to 23°45′N. *Journal of Petrology*, *51*, 425–467. https://doi.org/10.1093/petrology/egp088

Dick, H. J. B. (1989). Abyssal peridotites, very slow spreading ridges and ocean ridge magmatism. *Geological Society, London, Special Publications*, *42*(1), 71–105. https://doi.org/10.1144/GSL.SP.1989.042.01.06

Dijkstra, A. H., Sergeev, D. S., Spandler, C., Pettke, T., Meisel, T., & Cawood, P. A. (2010). Highly refractory peridotites on Macquarie Island and the case for anciently depleted domains in the Earth's mantle. *Journal of Petrology*, *51*, 469–493. https://doi.org/10.1093/petrology/egp084

Direen, N. G., Stagg, H. M., Symonds, P. A., & Colwell, J. B. (2011). Dominant symmetry of a conjugate southern Australian and East Antarctic magma–poor rifted margin segment. *Geochemistry, Geophysics, Geosystems*, *12*, Q03006. https://doi.org/10.1029/2010GC003306

Direen, N. G., Stagg, H. M., Symonds, P. A., & Norton, I. O. (2013). Variations in rift symmetry: Cautionary examples from the southern rift system (Australia–Antarctica). *Geological Society, London, Special Publications*, *369*, 453–475. https://doi.org/10.1144/SP369.4

Donovan, J. J., & Tingle, T. N. (1996). An improved mean atomic number correction for quantitative microanalysis. *Journal of Microscopy*, *2*(1), 1–7. https://doi.org/10.1017/S1431927696210013

Downes, H. (2007). Origin and significance of spinel and garnet pyroxenites in the shallow lithospheric mantle: Ultramafic massifs in orogenic belts in Western Europe and NW Africa. *Lithos*, *99*, 1–24. https://doi.org/10.1016/j.lithos.2007.05.006

Drouin, M., Godard, M., Ildefonse, B., Bruguier, O., & Garrido, C. J. (2009). Geochemical and petrographic evidence for magmatic impregnation in the oceanic lithosphere at Atlantis massif, mid-Atlantic ridge (IODP hole U1309D, 30°N). *Chemical Geology*, *264*, 71–88. https://doi.org/10.1016/j.chemgeo.2009.02.013

Dygert, N., & Liang, Y. (2015). Temperatures and cooling rates recorded in REE in coexisting pyroxenes in ophiolitic and abyssal peridotites. *Earth and Planetary Science Letters*, *420*, 151–161. https://doi.org/10.1016/j.epsl.2015.02.042

Eagles, G. (2019). A little spin in the Indian Ocean plate circuit. *Tectonophysics*, *754*, 80–100. https://doi.org/10.1016/j.tecto.2019.01.015

Elthon, D. (1992). Chemical trends in abyssal peridotites: Refertilisation of depleted suboceanic mantle. *Journal of Geophysical Research*, *97*(B6), 9015–9025. https://doi.org/10.1029/92JB0072

Epin, M. E., Manatschal, G., Amman, M., Ribes, C., Clausse, A., Guffon, T., & Lescanne, M. (2019). Polyphase tectono-magmatic evolution during mantle exhumation in an ultra-distal, magma-poor rift domain: Example of the fossil Platta ophiolite, SE Switzerland. *International Journal of Earth Sciences*, *108*, 1–25. https://doi.org/10.1007/s00531-019-01772-0

Feig, S., Koepke, J., & Snow, E. J. (2006). Effect of water on tholeiitic basalt phase equilibria: An experimental study under oxidizing conditions. *Contributions to Mineralogy and Petrology*, *152*, 611–638. https://doi.org/10.1007/s00410-006-0123-2

Florineth, D., & Froitzheim, N. (1994). Transition from continental to oceanic basement in the Tasna nappe (Engadine window, Graubunden, Switzerland): Evidence for early cretaceous opening of the Valais Ocean. *Schweizerische Mineralogische und Petrographische Mitteilungen*, *74*, 437–448.

Forsyth, D. W., Ehrenbard, R. L., & Chapin, S. (1987). Anomalous upper mantle beneath the Australian-Antarctic Discordance. *Earth and Planetary Science Letters*, *84*(4), 471–478. https://doi.org/10.1016/0012-821X(87)90011-2

Franke, D. (2013). Rifting, lithosphere breakup and volcanism: Comparison of magma-poor and volcanic rifted margins. *Marine and Petroleum Geology*, *43*, 63–87. https://doi.org/10.1016/j.marpetgeo.2012.11.003

Frey, F. A., & Green, D. H. (1974). The mineralogy, geochemistry and origin of lherzolite inclusions in Victorian basanites. *Geochimica et Cosmochimica Acta*, *38*(7), 1023–1059. https://doi.org/10.1016/0016-7037(74)90003-9

Frey, F. A., Green, D. H., & Roy, S. D. (1978). Integrated models of basalt petrogenesis—A study of quartz tholeiites to olivine melilitites from southeastern Australia utilizing geochemical and experimental petrological data. *Journal of Petrology*, *19*(3), 463–513. https://doi.org/10.1093/petrology/19.3.463

Fumagalli, P., Borghini, G., Rampone, E., & Poli, S. (2017). Experimental calibration of Forsterite–Anorthite–Ca-Tschermak–Enstatite (FACE) geobarometer for mantle peridotites. *Contributions to Mineralogy and Petrology*, *172*. https://doi.org/10.1007/s00410-017-1352-2

Gillard, M., Autin, J., & Manatschal, G. (2016). Fault systems at hyper-extended rifted margins and embryonic oceanic crust: Structural style, evolution and relation to magma. *Marine and Petroleum Geology*, *76*, 51–67. https://doi.org/10.1016/j.marpetgeo.2016.05.013

Gillard, M., Autin, J., Manatschal, G., Sauter, D., Munschy, M., & Schaming, M. (2015). Tectonomagmatic evolution of the final stages of rifting along the deep conjugate Australian-Antarctic magma-poor rifted margins: Constraints from seismic observations. *Tectonics*, *34*, 753–783. https://doi.org/10.1002/2015TC003850

Golynsky, A. V., Ferraccioli, F., Hong, J. K., Golynsky, D. A., von Frese, R. R. B., Young, D. A., et al. (2018). New magnetic anomaly map of the Antarctic. *Geophysical Research Letters*, *45*, 6437–6449. https://doi.org/10.1029/2018GL078153

Golynsky, A. V., Ivanov, S. V., Kazankov, A. J., Jokat, W., Masolov, V. N., & von Frese, R. R. B. (2012). New continental margin magnetic anomalies of East Antarctica. *Tectonophysics*, *585*, 172–184. https://doi.org/10.1016/j.tecto.2012.06.043

Green, D. H. (1963). Alumina content of enstatite in a Venezuelan high temperature peridotite. *Geological Society of America Bulletin*, *74*(11), 1397–1402. https://doi.org/10.1130/0016-7606(1963)74[1397:ACOEIA]2.0.CO;2

Green, D. H. (1964). The petrogenesis of the high-temperature peridotite intrusion in the Lizard area, Cornwall. *Journal of Petrology*, *5*(1), 134–188. https://doi.org/10.1093/petrology/5.1.134

Green, D. H., & Ringwood, A. E. (1967). The genesis of basaltic magmas. *Contributions to Mineralogy and Petrology*, *15*(2), 103–190. https://doi.org/10.1007/BF00372052

Grove, T. L., Kinzler, R. J., & Bryan, W. B. (1992). Fractionation of mid-ocean ridge basalt (MORB). *Mantle flow and melt generation at mid-ocean ridges*, *71*, 281–310. https://doi.org/10.1029/GM071p0281

Gurnis, M., & Muller, R. D. (2003). Origin of the Australian-Antarctic Discordance from an ancient slab and mantle wedge. *Special Paper of the Geological Society of America*, *372*, 417–430. https://doi.org/10.1130/0-8137-2372-8.417

Herzberg, C. T. (1978). Pyroxene geothermometry and geobarometry: Experimental and thermodynamic evaluation of some subsolidus phase relations involving pyroxenes in the system CaO–MgO–Al_2O_3–SiO_2. *Geochimica et Cosmochimica Acta*, *42*(7), 945–957. https://doi.org/10.1016/0016-7037(78)90284-3

Holmes, R. C., Tolstoy, M., Harding, A. J., Orcutt, J. A., & Morgan, J. P. (2010). Australian Antarctic discordance as a simple mantle boundary. *Geophysical Research Letters*, *37*, L09309. https://doi.org/10.1029/2010GL042621

Husen, A., Almeev, R. R., & Holtz, F. (2016). The effect of H_2O and pressure on multiple saturation and liquid lines of descent in basalt from the Shatsky rise. *Journal of Petrology*, *57*, 309–344. https://doi.org/10.1093/petrology/egw008

Jacob, J., & Dyment, J. R. M. (2014). Early opening of Australia and Antarctica: New inferences and regional consequences. *Tectonophysics*, *636*, 244–256. https://doi.org/10.1016/j.tecto.2014.08.020

Jochum, K. P., & Stoll, B. I. (2008). Reference materials for elemental and isotopic analyses by LA-(MC)-ICP-MS: Successes and outstanding needs. In P. Sylvester (Ed.), *Laser ablation ICPMS in the earth sciences: Current practices and outstanding issues*, *Short Course*, (Vol. 40, pp. 147–168). Quebec: Mineralogical Association of Canada.

Johnson, K. T. M., Dick, H. J. B., & Shimizu, N. (1990). Melting in the oceanic upper mantle: An ion microprobe study of diopsides in abyssal peridotites. *Journal of Geophysical Research*, *95*(B3), 2661–2678. https://doi.org/10.1029/JB095iB03p02661

Kaczmarek, M.-A., & Müntener, O. (2008). Juxtaposition of melt impregnation and high-temperature shear zones in the upper mantle; field and petrological constraints from the Lanzo Peridotite (Northern Italy). *Journal of Petrology*, *49*, 2187–2220. https://doi.org/10.1093/petrology/egn065

Kaus, B. J., Connolly, J. A., Podladchikov, Y. Y., & Schmalholz, S. M. (2005). Effect of mineral phase transitions on sedimentary basin subsidence and uplift. *Earth and Planetary Science Letters*, *233*, 213–228. https://doi.org/10.1016/j.epsl.2005.01.032

Lagabrielle, Y., Brovarone, A. V., & Ildefonse, B. (2015). Fossil oceanic core complexes recognized in the blueschist metaophiolites of Western Alps and Corsica. *Earth-Science Reviews*, *141*, 1–26. https://doi.org/10.1016/j.earscirev.2014.11.004

Lagabrielle, Y., & Cannat, M. (1990). Alpine Jurassic ophiolites resemble the modern central Atlantic basement. *Geology*, *18*, 319–322. https://doi.org/10.1130/0091-7613(1990)018<0319:AJORTM>2.3.CO;2

Lagabrielle, Y., & Lemoine, M. (1997). Alpine Corsican and Apennine ophiolites: The slow-spreading ridge model. *Comptes Rendus de l'Académie des Sciences - Series IIA - Earth and Planetary Science*, *325*(12), 909–920. https://doi.org/10.1016/S1251-8050(97)82369-5

Larsen, H. C., Mohn, G., Nirrengarten, M., Sun, Z., Stock, J., Jian, Z., et al. (2018). Rapid transition from continental breakup to ocean crust at South China Sea rifted margin. *Nature Geoscience*, *11*, 782–789. https://doi.org/10.1038/s41561-018-0198-1

Laukert, G., von der Handt, A., Hellebrand, E., Snow, J. E., Hoppe, P., & Klügel, A. (2014). High-pressure reactive melt stagnation recorded in abyssal pyroxenites from the ultraslow-spreading Lena trough, Arctic Ocean. *Journal of Petrology*, *55*, 427–458. https://doi.org/10.1093/petrology/egt073

Lavin, C. (1997). The Maastrichtian breakup of the Otway Basin margin—A model developed by integrating seismic interpretation, sequence statigraphy and thermochronological studies. *Exploration Geophysics*, *28*(1–2), 252–259. https://doi.org/10.1071/EG997252

Le Pichon, X., & Heirtzler, J. R. (1968). Magnetic anomalies in the Indian Ocean and sea-floor spreading. *Journal of Geophysical Research*, *73*(6), 2101–2117. https://doi.org/10.1029/JB073i006p02101

Le Roux, V., Bodinier, J.-L., Tommasi, A., Alard, O., Dautria, J.-M., Vauchez, A., & Riches, A. J. V. (2007). The Lherz spinel lherzolite: Refertilized rather than pristine mantle. *Earth and Planetary Science Letters*, *259*, 599–612. https://doi.org/10.1016/j.epsl.2007.05.026

Leake, B. E., Woolley, A. R., Arps, C. E., Birch, W. D., Gilbert, M. C., Grice, J. D., et al. (1997). Nomenclature of amphiboles; report of the subcommittee on amphiboles of the international mineralogical association commission on new minerals and mineral names. *Mineralogical Magazine*, *61*(405), 295–310. https://doi.org/10.1180/minmag.1997.061.405.13

Leitchenkov, G., Gandyukhin, V., Guseva, Y., and Kazankov, A., (2007). Crustal structure and evolution of the Mawson Sea, western Wilkes Land margin, East Antarctica. In: Cooper, A. K., Raymond, C. R. (Eds.), *Antarctica: A keystone in a changing world*, Reston, VA: U.S. Geological Survey. Online Proceedings for the Tenth International Symposium on Antarctic Earth Sciences. USGS Open-File Report 1047, https://doi.org/10.3133/ofr20071047SRP028

Leitchenkov, G. L., Guseva, Y. B., Gandyukhin, V. V., & Ivanov, S. V. (2015). *In Russian. Crustal Structure, Tectonic Evolution and Seismic Stratigraphy of the Southern Indian Ocean/СТРОЕНИЕ ЗЕМНОЙ КОРЫ И ИСТОРИЯ ГЕОЛОГИЧЕСКОГО РАЗВИТИЯ ОСАДОЧНЫХ БАССЕЙНОВ ИНДООКЕАНСКОЙ АКВАТОРИИ АНТАРКТИКИ*. St. Petersburg: Academy Publishing Center. ISBN: 978-5-88994-117-0.

Leuthold, J., Lissenberg, C. J., O'Driscoll, B., Karakas, O., Falloon, T., Klimentyeva, D. N., & Ulmer, P. (2018). Partial melting of lower oceanic crust gabbro: Constraints from poikilitic clinopyroxene primocrysts. *Frontiers in Earth Science*, *6*, 15. https://doi.org/10.3389/feart.2018.00015

Liang, Y., Sun, C., & Yao, L. (2013). A REE-in-two-pyroxene thermometer for mafic and ultramafic rocks. *Geochimica et Cosmochimica Acta*, *102*, 246–260. https://doi.org/10.1016/j.gca.2012.10.035

Lissenberg, C. J., & Dick, H. J. (2008). Melt–rock reaction in the lower oceanic crust and its implications for the genesis of mid-ocean ridge basalt. *Earth and Planetary Science Letters*, *271*, 311–325. https://doi.org/10.1016/j.epsl.2008.04.023

Maffione, M., Morris, A., Plümper, O., & van Hinsbergen, D. J. J. (2014). Magnetic properties of variably serpentinized peridotites and their implication for the evolution of oceanic core complexes. *Geochemistry, Geophysics, Geosystems*, *15*, 923–944. https://doi.org/10.1002/2013GC004993

Manatschal, G. (2004). New models for evolution of magma-poor rifted margins based on a review of data and concepts from West Iberia and the Alps. *International Journal of Earth Sciences*, *93*, 432–466. https://doi.org/10.1007/s00531-004-0394-7

Manatschal, G., & Müntener, O. (2009). A type sequence across an ancient magma-poor ocean–continent transition: The example of the western Alpine Tethys ophiolites. *Tectonophysics*, *473*, 4–19. https://doi.org/10.1016/j.tecto.2008.07.021

Manatschal, G., & Nievergelt, P. (1997). A continent-ocean transition recorded in the Err and Platta nappes (Eastern Switzerland). *Eclogae Geologicae Helvetiae*, *90*(1), 3–28.

Manzotti, P., Ballèvre, M., Zucali, M., Robyr, M., & Engi, M. (2014). The tectonometamorphic evolution of the Sesia–dent Blanche nappes (internal Western Alps): Review and synthesis. *Swiss Journal of Geosciences*, *107*, 309–336. https://doi.org/10.1007/s00015-014-0172-x

Martin, A. P., Price, R. C., Cooper, A. F., & McCammon, C. A. (2014). Petrogenesis of the rifted southern Victoria Land lithospheric mantle, Antarctica, inferred from petrography, geochemistry, thermobarometry and oxybarometry of peridotite and pyroxenite xenoliths from the mount morning eruptive centre. *Journal of Petrology*, *56*, 193–226. https://doi.org/10.1093/petrology/egu075

Masaaki, O. (1980). The Ronda peridotite: Garnet-, spinel-, and plagioclase-lherzolite facies and the *PT* trajectories of a high-temperature mantle intrusion. *Journal of Petrology*, *21*(3), 533–572. https://doi.org/10.1093/petrology/21.3.533

Matthews, D. H., & Bath, J. (1967). Formation of magnetic anomaly pattern of Mid-Atlantic Ridge. *Geophysical Journal International*, *13*(1–3), 349–357. https://doi.org/10.1111/j.1365-246X.1967.tb02165.x

McCarthy, A., & Müntener, O. (2015). Ancient depletion and mantle heterogeneity: Revisiting the Permian-Jurassic paradox of Alpine peridotites. *Geology*, *43*, 255–258. https://doi.org/10.1130/G36340.1

McCarthy, A., & Müntener, O. (2019). Evidence for ancient fractional melting, cryptic refertilization and rapid exhumation of Tethyan mantle (Civrari Ophiolite, NW Italy). *Contributions to Mineralogy and Petrology*, *174*, 69. https://doi.org/10.1007/s00410-019-1603-5

McDonough, W. F., & Sun, S. S. (1995). The composition of the earth. *Chemical Geology*, *120*(3-4), 223–253. https://doi.org/10.1016/0009-2541(94)00140-4

McKenzie, D. (1978). Some remarks on the development of sedimentary basins. *Earth and Planetary Science Letters*, *40*(1), 25–32. https://doi.org/10.1016/0012-821x(78)90071-7

Menzies, M. A., & Dupuy, C. (1991). Orogenic massifs: Protolith, process and provenance. *Journal of Petrology*, *Special_Volume*(2), 1–16. https://doi.org/10.1093/petrology/Special_Volume.2.1

Merle, R., Kaczmarek, M.-A., Tronche, E., & Girardeau, J. (2012). Occurrence of inherited supra-subduction zone mantle in the oceanic lithosphere as inferred from mantle xenoliths from Dragon Seamount (southern Tore–Madeira Rise). *Journal of the Geological Society, London*, *169*, 251–267. https://doi.org/10.1144/0016-76492011-015

Minakov, A. N., & Podladchikov, Y. Y. (2012). Tectonic subsidence of the Lomonosov Ridge. *Geology*, *40*, 99–102. https://doi.org/10.1130/G32445.1

Montanini, A., Tribuzio, R., & Anczkiewicz, R. (2006). Exhumation history of a garnet pyroxenite-bearing mantle section from a continent–ocean transition (Northern Apennine ophiolites, Italy). *Journal of Petrology*, *47*, 1943–1971. https://doi.org/10.1093/petrology/egl032

Montanini, A., Tribuzio, R., & Vernia, L. (2008). Petrogenesis of basalts and gabbros from an ancient continent–ocean transition (External Liguride ophiolites, Northern Italy). *Lithos*, *101*, 453–479. https://doi.org/10.1016/j.lithos.2007.09.007

Müntener, O., Hermann, J., & Trommsdorff, V. (2000). Cooling history and exhumation of lower-crustal granulite and upper mantle (Malenco, Eastern Central Alps). *Journal of Petrology*, *41*(2), 175–200. https://doi.org/10.1093/petrology/41.2.175

Müntener, O., & Manatschal, G. (2006). High degrees of melt extraction recorded by spinel harzburgite of the Newfoundland margin: The role of inheritance and consequences for the evolution of the southern North Atlantic. *Earth and Planetary Science Letters*, *252*, 437–452. https://doi.org/10.1016/j.epsl.2006.10.009

Müntener, O., Manatschal, G., Desmurs, L., & Pettke, T. (2010). Plagioclase peridotites in ocean–continent transitions: Refertilized mantle domains generated by melt stagnation in the shallow mantle lithosphere. *Journal of Petrology*, *51*, 255–294. https://doi.org/10.1093/petrology/egp087

Müntener, O., & Piccardo, G. B. (2003). Melt migration in ophiolitic peridotites: The message from Alpine-Apennine peridotites and implications for embryonic ocean basins. *Geological Society, London, Special Publications*, *218*(1), 69–89. https://doi.org/10.1144/GSL.SP.2003.218.01.05

Müntener, O., Pettke, T., Desmurs, L., Meier, M., & Schaltegger, U. (2004). Refertilization of mantle peridotite in embryonic ocean basins: trace element and Nd isotopic evidence and implications for crust–mantle relationships. *Earth and Planetary Science Letters*, *221*, 293–308.

Nicholls, I. A., Ferguson, J., Jones, H., Marks, G. P., & Mutter, J. C. (1981). Ultramafic blocks from the ocean floor southwest of Australia. *Earth and Planetary Science Letters*, *56*, 362–374. https://doi.org/10.1016/0012-821X(81)90140-0

Nickel, K. G., & Green, D. H. (1984). The nature of the upper-most mantle beneath Victoria, Australia as deduced from UL tramafic xenoliths. *Developments in Petrology*, *11*(2), 161–178. https://doi.org/10.1016/B978-0-444-42274-3.50020-2

Niida, K., & Green, D. H. (1999). Stability and chemical composition of pargasitic amphibole in MORB pyrolite under upper mantle conditions. *Contributions to Mineralogy and Petrology*, *135*(1), 18–40. https://doi.org/10.1007/s004100050495

Niida, K., & Yuasa, M. (1995). Peridotites from the seamount off Wilkes Land, Antarctica. *Proc. NIPR Symposium Antarctic Geoscience*, *8*, 169–180.

Nirrengarten, M., Manatschal, G., Tugend, J., Kusznir, N., & Sauter, D. (2018). Kinematic evolution of the southern North Atlantic: Implications for the formation of hyper-extended rift systems. *Tectonics*, *37*, 89–118. https://doi.org/10.1002/2017TC004495

Norman, M. D. (1998). Melting and metasomatism in the continental lithosphere: Laser ablation ICPMS analysis of minerals in spinel lherzolites from eastern Australia. *Contributions to Mineralogy and Petrology*, *130*(3–4), 240–255. https://doi.org/10.1007/s004100050363

Panjasawatwong, Y., Danyushevsky, L. V., Crawford, A. J., & Harris, K. L. (1995). An experimental study of the effects of melt composition on plagioclase-melt equilibria at 5 and 10 kbar: Implications for the origin of magmatic high-An plagioclase. *Contributions to Mineralogy and Petrology*, *118*(4), 420–432. https://doi.org/10.1007/s004100050024

Picazo, S., Müntener, O., Manatschal, G., Bauville, A., Karner, G., & Johnson, C. (2016). Mapping the nature of mantle domains in Western and Central Europe based on clinopyroxene and spinel chemistry: Evidence for mantle modification during an extensional cycle. *Lithos*, *266-267*, 233–263. https://doi.org/10.1016/j.lithos.2016.08.029

Piccardo, G. B., Vannucci, R., & Guarnirei, L. (2009). Evolution of the lithospheric mantle in an extensional setting: Insights from ophiolitic peridotites. *Lithosphere*, *1*, 81–87. https://doi.org/10.1130/L30.1

Piccardo, G. B., Zanetti, A., & Müntener, O. (2007). Melt/peridotite interaction in the southern Lanzo peridotite: Field, textural and geochemical evidence. *Lithos*, *94*, 181–209. https://doi.org/10.1016/j.lithos.2006.07.002

Pitman, W. C., & Heirtzler, J. R. (1966). Magnetic anomalies over the Pacific-Antarctic Ridge. *Science*, *154*(3753), 1164–1171. https://doi.org/10.1126/science.154.3753.1164

Powell, C. M., Roots, S. R., & Veevers, J. J. (1988). Pre-breakup continental extension in east Gondwanaland and the early opening of the eastern Indian Ocean. *Tectonophysics*, *155*(1–4), 261–283. https://doi.org/10.1016/0040-1951(88)90269-7

Presnall, D. C. (1976). Alumina content of enstatite as a geobarometer for plagioclase and spinel lherzolites. *American Mineralogist*, *61*(7–8), 582–588.

Rampone, E., & Hofmann, A. W. (2012). A global overview of isotopic heterogeneities in the oceanic mantle. *Lithos*, *148*, 247–261. https://doi.org/10.1016/j.lithos.2012.06.018

Rampone, E., Hofmann, A. W., & Raczek, I. (1998). Isotopic contrasts within the Internal Liguride ophiolite (N. Italy): The lack of a genetic mantle–crust link. *Earth and Planetary Science Letters*, *163*(1–4), 175–189. https://doi.org/10.1016/S0012-821X(98)00185-X

Rampone, E., Piccardo, G. B., & Hofmann, A. W. (2008). Multi-stage melt–rock interaction in the Mt. Maggiore (Corsica, France) ophiolitic peridotites: Microstructural and geochemical evidence. *Contributions to Mineralogy and Petrology*, *156*, 453–475. https://doi.org/10.1007/s00410-008-0296-y

Rampone, E., Piccardo, G. B., Vannucci, R., Bottazzi, P., & Ottolini, L. (1993). Subsolidus reactions monitored by trace element partitioning: The spinel- to plagioclasi-facies transition in mantle peridotites. *Contributions to Mineralogy and Petrology*, *115*(1), 1–17. https://doi.org/10.1007/BF00712974

Renna, M. R., & Tribuzio, R. (2011). Olivine-rich troctolites from Ligurian ophiolites (Italy): Evidence for impregnation of replacive mantle conduits by MORB-type melts. *Journal of Petrology*, *52*, 1763–1790. https://doi.org/10.1093/petrology/egr029

Renna, M. R., Tribuzio, R., & Ottolini, L. (2016). New perspectives on the origin of olivine-rich troctolites and associated harrisites from the Ligurian ophiolites (Italy). *Journal of the Geological Society*, *173*, 916–932. https://doi.org/10.1144/jgs2015-135

Sanfilippo, A., Dick, H. J., & Ohara, Y. (2013). Melt–rock reaction in the mantle: Mantle troctolites from the Parece Vela ancient back-arc spreading center. *Journal of Petrology*, *54*, 861–885. https://doi.org/10.1093/petrology/egs089

Sanfilippo, A., Salters, V., Tribuzio, R., & Zanetti, A. (2019). Role of ancient, ultra-depleted mantle in Mid-Ocean-Ridge magmatism. *Earth and Planetary Science Letters*, *511*, 89–98. https://doi.org/10.1016/j.epsl.2019.01.018

Sayers, J., Symonds, P. A., Direen, N. G., & Bernadel, G. (2001). Nature of the continent-ocean transition on the non-volcanic rifted margin in the central Great Australian Bight. In R. C. L. Wilson, R. B. Whitmarsh, B. Taylor, & N. Froitzheim (Eds.), *Non-volcanic rifting of continental margins: A comparison of evidence from land and sea*, (Vol. 187, pp. 51–76). London: Geological Society, Special Publications.

Seton, M., Whittaker, J. M., Wessel, P., Müller, R. D., DeMets, C., Merkouriev, S., et al. (2014). Community infrastructure and repository for marine magnetic identifications. *Geochemistry, Geophysics, Geosystems*, *15*, 1629–1641. https://doi.org/10.1002/2013GC005176

Simon, N. S., & Podladchikov, Y. Y. (2008). The effect of mantle composition on density in the extending lithosphere. *Earth and Planetary Science Letters*, *272*, 148–157. https://doi.org/10.1016/j.epsl.2008.04.027

Stagg, H. M. J. and Reading, A. M., (2007). Crustal architecture of the oblique-slip conjugate margins of George V Land and Southeast Australia. In: Proceedings of Antarctica: A Keystone in a Changing World. Online Proceedings for the 10th International Symposium on Antarctic Earth Sciences. US Geological Survey, Open-File Report, 1047: *109*, 1–6. https://doi.org/10.3133/of2007-1047.srp109

Suhr, G., Hellebrand, E., Johnson, K., & Brunelli, D. (2008). Stacked gabbro units and intervening mantle: A detailed look at a section of IODP Leg 305, Hole U1309D. *Geochemistry, Geophysics, Geosystems*, *9*, Q10007. https://doi.org/10.1029/2008GC002012

Tanahashi, M., Ishihara, T., Yuasa, M., Murakami, F., & Nishimura, A. (1997). Preliminary report of the TH95 geological and geophysical survey results in the Ross Sea and Dumont D'Urville Sea. *Proc. NIPR Symposium, Antarctic Geoscience*, *10*, 36–58.

Tikku, A. A., & Cande, S. C. (2000). On the fit of Broken Ridge and Kerguelen plateau. *Earth and Planetary Science Letters*, *180*(1-2), 117–132. https://doi.org/10.1016/S0012-821X(00)00157-6

Tikku, A. A., & Candes, S. C. (1999). The oldest magnetic anomalies in the Australian-Antarctic Basin: Are they isochrons? *Journal of Geophysical Research*, *104*(B1), 661–677. https://doi.org/10.1029/1998JB900034

Tikku, A. A., & Direen, N. H. (2008). Comment on "Major Australian-Antarctic Plate Reorganization at Hawaiian-Emperor Bend Time". *Science*, 490c, *321*, 490. https://doi.org/10.1126/science.1157163

Totterdell, J. M., Blevin, J. E., Struckmeyer, H. I. M., Bradshaw, B. E., Colwell, J. B., & Kennard, J. M. (2000). A new sequence framework for the Great Australian Bight: Starting with a clean slate. *The APPEA Journal*, *40*(1), 95–118. https://doi.org/10.1071/AJ99007

Vannucci, R., Piccardo, G. B., Rivalenti, G., Zanetti, A., Rampone, E., Ottolini, L., et al. (1995). Origin of LREE-depleted amphiboles in the subcontinental mantle. *Geochimica et Cosmochimica Acta*, *59*(9), 1763–1771. https://doi.org/10.1016/0016-7037(95)00080-J

Veevers, J. J. (1982). Australian–Antarctic depression from the mid-ocean ridge to adjacent continents. *Nature*, *295*(5847), 315–317. https://doi.org/10.1038/295315a0

Veevers, J. J. (1986). Breakup of Australia and Antarctica estimated as mid-Cretaceous (95±5 Ma) from magnetic and seismic data at the continental margin. *Earth and Planetary Science Letters*, *77*(1), 91–99. https://doi.org/10.1016/0012-821X(86)90135-4

Villiger, S., Ulmer, P., & Müntener, O. (2007). Equilibrium and fractional crystallization experiments at 0·7 GPa; the effect of pressure on phase relations and liquid compositions of tholeiitic magmas. *Journal of Petrology*, *48*(1), 159–184. https://doi.org/10.1093/petrology/egl058

Vine, F. J., & Matthews, D. H. (1963). Magnetic anomalies over oceanic ridges. *Nature*, *199*(4897), 947–949. https://doi.org/10.1038/199947a0

Vissers, R. L., van Hinsbergen, D. J., Meijer, P. T., & Piccardo, G. B. (2013). Kinematics of Jurassic ultra-slow spreading in the Piemonte Ligurian Ocean. *Earth and Planetary Science Letters*, *380*, 138–150. https://doi.org/10.1016/j.epsl.2013.08.033

Wardell, N., Childs, J. R., and Cooper, A. K., (2007). Advances through collaboration: Sharing seismic reflection data via the Antarctic Seismic Data Library System for Cooperative Research (SDLS), in Antarctica: A Keystone in a Changing World - Online Proceedings of

the 10th ISAES.. In A. K. Cooper et al. (Eds.), *USGS Open-File Report 2007–1047, Short Research Paper001* (4 p). Reston, VA: U.S. Geological Survey. https://doi.org/10.3133/of2007-1047.srp001

Warren, J. M. (2016). Global variations in abyssal peridotite compositions. *Lithos*, *248-251*, 193–219. https://doi.org/10.1016/j.lithos.2015.12.023

Warren, J. M., Shimizu, N., Sakaguchi, C., Dick, H. J. B., & Nakamura, E. (2009). An assessment of upper mantle heterogeneity based on abyssal peridotite isotopic compositions. *Journal of Geophysical Research*, *114*, B12203. https://doi.org/10.1029/2008JB006186

Weissel, J. K., & Hayes, D. E. (1972). Magnetic anomalies in the Southeast Indian Ocean. In D. E. Hayes (Ed.), *Antarctica Oceanology II: The Australian–New Zealand Sector*, (pp. 165–196). Washington, D. C.: AGU. https://doi.org/10.1029/AR019p0165

White, L., Gibson, G., & Lister, G. (2013). A reassessment of paleogeographic reconstructions of eastern Gondwana: Bringing geology back into the equation. *Gondwana Research*, *24*, 984–998. https://doi.org/10.1016/j.gr.2013.06.009

Whitmarsh, R. B., Manatschal, G., & Minshull, T. A. (2001). Evolution of magma-poor continental margins from rifting to sea-floor spreading. *Nature*, *413*(6852), 150–154. https://doi.org/10.1038/35093085

Whitney, D. L., & Evans, B. W. (2010). Abbreviations for names of rock-forming minerals. *American Mineralogist*, *95*, 185–187. https://doi.org/10.2138/am.2010.3371

Whittaker, J. M., Müller, R. D., & Gurnis, M. (2010). Development of the Australian-Antarctic depth anomaly. *Geochemistry, Geophysics, Geosystems*, *11*, Q11006. https://doi.org/10.1029/2010GC003276

Whittaker, J. M., Müller, R. D., Leitchenkov, G., Stagg, H., Sdrolias, M., Gaina, C., & Goncharov, A. (2007). Major Australian-Antarctic plate reorganization at Hawaiian-Emperor bend time. *Science*, *318*, 83–86. https://doi.org/10.1126/science.1143769

Whittaker, J. M., Williams, S. E., & Müller, R. D. (2013). Revised tectonic evolution of the eastern Indian Ocean. *Geochemistry, Geophysics, Geosystems*, *14*, 1891–1909. https://doi.org/10.1002/ggge.20120

Williams, S. E., Whittaker, J. M., Halpin, J. A., & Müller, R. D. (2019). Australian-Antarctic break up and seafloor spreading: Balancing geological and geophysical constraints. *Earth-Science Reviews*, *188*, 41–58. https://doi.org/10.1016/j.earscirev.2018.10.011

Williams, S. E., Whittaker, J. M., & Müller, R. D. (2011). Full-fit, palinspastic reconstruction of the conjugate Australian-Antarctic margins. *Tectonics*, *30*, TC6012. https://doi.org/10.1029/2011TC002912

Williams, S.E., Whittaker, J.M., Müller, R.D., (2012). Full-fit reconstructions of the southern Australian margin and Antarctica—Implications for correlating geology between Australia and Antarctica, Proceedings of the Eastern Australasian Basins Symposium IV, Brisbane Qld

Workman, R. K., & Hart, S. R. (2005). Major and trace element composition of the depleted MORB mantle (DMM). *Earth and Planetary Science Letters*, *231*, 53–72. https://doi.org/10.1016/j.epsl.2004.12.005

Yuasa, M., Niida, K., Ishihara, T., Kisimoto, K., & Murakami, F. (1997). Peridotite dredged from a seamount off Wilkes Land, the Antarctic: Emplacement of fertile mantle fragment at early rifting stage between Australia and Antarctica during the final breakup of Gondwanaland. In *The Antarctic Region: Geological evolution and processes*, (pp. 725–730). Terra Antarctica: Siena. ISBN:8890022108.